Insights into spatial sensitivities of ice mass response to environmental change from the SeaRISE ice sheet modeling project I: Antarctica

Sophie Nowicki,[1] Robert A. Bindschadler,[1] Ayako Abe-Ouchi,[2] Andy Aschwanden,[3] Ed Bueler,[3] Hyeungu Choi,[4] Jim Fastook,[5] Glen Granzow,[6] Ralf Greve,[7] Gail Gutowski,[8] Ute Herzfeld,[9] Charles Jackson,[8] Jesse Johnson,[6] Constantine Khroulev,[3] Eric Larour,[10] Anders Levermann,[11] William H. Lipscomb,[12] Maria A. Martin,[11] Mathieu Morlighem,[13] Byron R. Parizek,[14] David Pollard,[15] Stephen F. Price,[12] Diandong Ren,[16] Eric Rignot,[10,13] Fuyuki Saito,[17] Tatsuru Sato,[7] Hakime Seddik,[7] Helene Seroussi,[10] Kunio Takahashi,[17] Ryan Walker,[1,18] and Wei Li Wang[1]

Received 28 July 2012; revised 12 April 2013; accepted 23 April 2013; published 12 June 2013.

[1] Atmospheric, oceanic, and subglacial forcing scenarios from the Sea-level Response to Ice Sheet Evolution (SeaRISE) project are applied to six three-dimensional thermomechanical ice-sheet models to assess Antarctic ice sheet sensitivity over a 500 year timescale and to inform future modeling and field studies. Results indicate (i) growth with warming, except within low-latitude basins (where inland thickening is outpaced by marginal thinning); (ii) mass loss with enhanced sliding (with basins dominated by high driving stresses affected more than basins with low-surface-slope streaming ice); and (iii) mass loss with enhanced ice shelf melting (with changes in West Antarctica dominating the signal due to its marine setting and extensive ice shelves; cf. minimal impact in the Terre Adelie, George V, Oates, and Victoria Land region of East Antarctica). Ice loss due to dynamic changes associated with enhanced sliding and/or sub-shelf melting exceeds the gain due to increased precipitation. Furthermore, differences in results between and within basins as well as the controlling impact of sub-shelf melting on ice dynamics highlight the need for improved understanding of basal conditions, grounding-zone processes, ocean-ice interactions, and the numerical representation of all three.

Citation: Nowicki, S., et al. (2013), Insights into spatial sensitivities of ice mass response to environmental change from the SeaRISE ice sheet modeling project I: Antarctica, *J. Geophys. Res. Earth Surf.*, *118*, 1002–1024, doi:10.1002/jgrf.20081.

1. Introduction

[2] Antarctica contains 70% of the world's fresh water, which represents a potential 56.6 m of sea level rise [*IPCC*, 2007] if all its ice were to melt. Over the past decades, rapid and dramatic changes have been observed in Antarctica: spectacular collapses of several ice shelves in the Antarctic Peninsula [*Scambos et al.*, 2004, 2009] and the acceleration

Additional supporting information may be found in the online version of this article.

This article is a companion to Nowicki et al. [2013] doi:10.1002/jgrf.20076.

[1]Code 615, NASA Goddard Space Flight Center, Greenbelt, Maryland, USA.
[2]Atmosphere and Ocean Research Institute, The University of Tokyo, Kashiwa, Chiba, Japan.
[3]Geophysical Institute, University of Alaska, Fairbanks, Arkansas, USA.
[4]Sigma Space Corporation, Lanham, Maryland, USA.
[5]Computer Science/Quaternary Institute, University of Maine, Orono, Maine, USA.
[6]College of Arts and Sciences, The University of Montana, Missoula, Montana, USA.
[7]Institute of Low Temperature Science, Hokkaido University, Sapporo, Japan.
[8]Institute for Geophysics, The University of Texas at Austin, Austin, Texas, USA.

Corresponding author: S. Nowicki, Code 615, NASA Goddard Space Flight Center, Greenbelt, MD 20771, USA. (sophie.nowicki@nasa.gov)

2169-9003/13/10.1002/jgrf.20081

[9]Department of Electrical, Computer and Energy Engineering and Cooperative Institute for Research in Environmental Sciences, University of Colorado, Boulder, Colorado, USA.
[10]Jet Propulsion Laboratory—California Institute of Technology, Pasadena, California, USA.
[11]Potsdam Institute for Climate Research, Potsdam, Germany.
[12]Los Alamos National Laboratory, Los Alamos, New Mexico, USA.
[13]Department of Earth System Science, University of California, Irvine, Irvine, California, USA.
[14]Mathematics and Geoscience, Penn State DuBois, College Place, DuBois, Pennsylvania, USA.
[15]Earth and Environmental Systems Institute, Pennsylvania State University, University Park, Pennsylvania, USA.
[16]Department of Physics, Curtin University of Technology, Perth, Australia.
[17]Japan Agency for Marine-Earth Science and Technology, Research Institute for Global Change, 3173-25 Showamachi, Kanazawa, Yokohama, Kanagawa, Japan.
[18]Earth System Science Interdisciplinary Center, University of Maryland, College Park, Maryland, USA.

of massive outlet glaciers such as Pine Island Glacier in the Amundsen Sea Embayment [*Rignot*, 2008]. Seven out of 12 ice shelves on the Antarctic Peninsula have significantly retreated or been almost entirely lost, and 87% of the 244 marine glacier fronts have retreated during the past 60 years [*Cook et al*., 2005]. These observed changes, thought to have been triggered by ocean warming and atmospheric changes [*Shepherd et al*., 2004; *Payne et al*., 2004; *Pritchard et al*., 2012], suggest that this ice sheet is far more vulnerable to climate change than initially anticipated by the Fourth Assessment Report of the Intergovernmental Panel on Climate Change (IPCC AR4) [*IPCC*, 2007]. The IPCC AR4 sea level rise projections for the year 2100, which ranged from 0.18 to 0.58 m, were acknowledged to be conservative, as these values excluded "future dynamical changes in ice sheet flow," because no ice sheet model could reproduce the recently observed changes occurring on the Greenland and Antarctic ice sheets.

[3] The IPCC AR4 conclusions triggered a number of workshops to discuss improvements in the capability of existing ice sheet models [*Little et al*., 2007; *Oppenheimer et al*., 2007; *Lipscomb et al*., 2009; *van der Veen and ISMASS*, 2010] and in particular how to incorporate the processes driving the observed rapid changes. Improving ice sheet models, however, takes time, as it requires an understanding of the key processes that are observed, in tandem with theoretical and numerical studies in order to develop and implement new parameterizations of the subgrid relevant processes that are to be incorporated in continental ice sheet models. Thus, modeling of the Antarctic ice sheet remains a technical and scientific challenge [*Vaughan and Arthern*, 2007; *Alley and Joughin*, 2012] given the size of the continent, the numerous physical processes that need to be accounted for and are not always well understood, and the lack of observational data. Climate models face similar challenges, yet the possible range of climate response to various future scenarios can still be examined through the analysis of results from multiple models [*IPCC*, 2007].

[4] The Sea-level Response to Ice Sheet Evolution effort (SeaRISE) seeks to investigate the sensitivity and the potential future response of the Antarctic and Greenland ice sheets for the coming 500 years. SeaRISE is not a model development effort but occurred in parallel to improvement in continental ice sheet models [e.g., *Bueler and Brown*, 2009; *Larour et al*., 2012a; *Seddik et al*., 2012; *Price et al*., 2011]. SeaRISE started in 2008 with the assumption that when projecting the evolution of continental scale ice sheets in response to various external climatic forcings, there is currently no "best" model, so that more can be learned about the sensitivity of the actual ice sheets from the projected response of many models, which follows from the findings of the climate modeling community. In particular, when multiple climate models are subjected to a set of common experiments, similar trends, as well as discrepancies, emerge from ensemble analysis [*Gates et al*., 1999; *Knutti et al*., 2010a] and can therefore guide where efforts are best spent to improve models and projections [*Knutti et al*., 2010b]. The strength of this approach lies in the use of a wide variety of models in the ensemble analysis, which allows for estimate of sensitivity to parameter change to be evaluated as broadly as possible. On the other hand, the weakness of such an approach lies in the difficulty of evaluating the absolute accuracy of each of the models involved and therefore of their aggregate ensemble projection.

[5] SeaRISE's strategy, as described in *Bindschadler et al*. [2013], is to therefore employ multiple models of ice sheet flow initialized by a common dataset to mitigate model-to-model differences and forced externally by a set of common climate scenarios. The data sets for the Antarctic ice sheet are available at http://websvr.cs.umt.edu/isis/index.php/Data and presented in *Bindschadler et al*. [2013]. This data include, for example, accumulation from observation [*Vaughan et al*., 1999; *Arthern et al*., 2006] or climate models [*van de Berg et al*., 2006], two basal heat fluxes [*Shapiro and Ritzwoller*, 2004; *Fox Maule et al*., 2005], along with surface elevation, basal topography, and ice thickness from ALBMAP v1 [*Le Brocq et al*., 2010]. As a primary goal was to involve as many ice sheet models as possible, the experiments were designed to be simple enough so that any model that was willing to contribute to SeaRISE could participate. The experiments investigated the response to three distinct forcings that are known to influence ice flow: (i) atmospheric forcing, modeled via changes in surface mass balance and temperature, (ii) oceanic forcing, modeled via changes in sub-shelf melt rate, and (iii) increased lubrication at the base of the ice sheet, modeled via enhanced basal sliding. For each forcing type, three different amplifications were investigated. Combinations of atmospheric, oceanic, and sliding forcings were also explored. The insight gained from these simple early experiments allowed SeaRISE to formulate a final experiment that attempts to model a more realistic future climate scenario (the R8 experiment in *Bindschadler et al*. [2013], which will be the focus of a different study). The six state-of-the-art ice sheet models taking part in the Antarctic suite of experiments are the Anisotropic Ice Flow model (AIF) [*Wang et al*., 2012], the Ice Sheet System Model (ISSM) [*Morlighem et al*., 2010; *Seroussi et al*., 2011; *Larour et al*., 2012a, 2012b], the PennState3D model [*Pollard and DeConto*, 2009, 2012], the Potsdam model [*Winkelmann et al*., 2011; *Martin et al*., 2011], the Simulation Code for Polythermal Ice Sheets model (SICOPOLIS) [*Greve*, 1997; *Sato and Greve*, 2012], and the University of Maine Ice Sheet Model (UMISM) [*Fastook*, 1990, 1993; *Fastook and Hughes*, 1990; *Fastook and Prentice*, 1994]. These models incorporate different sets of physical processes, ice flow approximations, and spatial resolutions, as well as different methods to implement the SeaRISE forcings, as summarized in Table A1 and in more detail in *Bindschadler et al*. [2013].

[6] *Bindschadler et al*. [2013] analyze the temporal response of the Antarctic and Greenland ice sheet volume, and hence sea-level contribution, for the various experiments. The atmospheric suite of experiment results in two types of behaviors for the Antarctic ice sheet: some models project a mass gain, while others suggest a mass loss. The un-weighted ensemble mean of all models (the mean resulting from a "one model, one vote" approach), suggests a growth of the Antarctic ice sheet associated with increased precipitation under warmer atmospheric conditions. The change in ice volume above flotation, which affects future

sea levels, is small compared to the oceanic or sliding suite of experiments. The increased basal velocities and sub-shelf melting result in an ice-sheet-wide mass loss for all models, with the oceanic forcing resulting in the largest contribution to sea level. In these two dynamic experiments, and for all amplifications, the fast rate of change in ice volume in the early stage of the simulated time period slows down over the duration of the 500 year simulation. Finally, *Bindschadler et al*. [2013] demonstrate that the temporal evolution of the ice sheet volume resulting from the combination experiment can be anticipated by combining the respective responses of the single-forcing experiments.

[7] The primary purpose of this paper is to investigate the spatial response of the Antarctic ice sheet to the SeaRISE forcings at specific times in order to gain insight into the changes in ice sheet wide volume reported in *Bindschadler et al*. [2013]. Our goal is to document improvements in experimental procedure or in ice sheet models that would benefit future modeling efforts such as SeaRISE. Here we focus on the spatial characteristics of the ice thickness as an ensemble un-weighted multi-model mean, rather than on individual model responses. A companion paper [*Nowicki et al*., 2013] repeats this analysis for the Greenland ice sheet. When combined with other statistical information such as standard deviation, the unweighted ensemble means not only capture the general trends but also identify where models agree or disagree [*Gates et al*., 1999]. The reasons for model disagreement are explored by analyzing the behaviors of the models that are the least sensitive and the most sensitive to the experiment. Although considering a subset of models, or weighting multi-model means, can improve the reliability of weather and climate predictions [e.g., *Stephenson et al*., 2005], evaluating the skill of models is difficult, as different metrics produce different rankings of the climate models considered [*Gleckler et al*., 2008]. The lack of a robust approach in assigning weights to climate models is problematic [*Knutti et al*., 2010a], as inappropriate weighting can lead to more information being lost than could potentially be gained by suitable weighting [*Weigel et al*., 2010]. In addition, focusing on specific model skills may lead to overconfidence and convergence that is unjustified [*Knutti et al*., 2010a]. When combining multi-model climate projections, *Knutti et al*. [2010a] therefore recommend in the first instance that all models be used in the ensemble without ranking or assigning weights. However, in acknowledgment that the ensemble approach hides the actual response of each model and that there is no guarantee that the ensemble trend is more likely than any single realization [e.g., *Giorgi*, 2005], the responses of all models are shown in the supporting information.

[8] The paper first presents the ice sheet models participating in the SeaRISE Antarctic experiments via a discussion, in section 2, of the initial conditions they used. The SeaRISE experiments are then described in section 3. The sensitivity of the Antarctic ice sheet to the simple SeaRISE forcings is presented in section 4 via a regional analysis of the change in ice volume and further explored in sections 5 with an analysis of the resulting spatial patterns of thickness change. The paper concludes in section 9, with a summary and discussion of the results presented and their implications for future forecasting efforts of sea-level from ice sheet models.

2. SeaRISE Experiments Initial Configurations

[9] The six whole ice sheet models taking part in the SeaRISE suite of Antarctic experiments obtain their starting configuration by either interglacial spin-up or data assimilation. Interglacial spin-up involves running a model through one or more interglacial cycles, which allows for fields such as internal temperature [*Rogozhina et al*., 2011] to be dependent on the long-term memory of the ice sheet, as timescales for thermal processes are of order 20 kyrs [*Huybrechts*, 1994]. The future evolution of an ice sheet initialized via interglacial spin-up therefore contains a natural transient due to the long-term climatic background evolution [e.g., *Huybrechts and de Wolde*, 1999]. However, as we demonstrate in this section, the end of spin-up configuration is often an ice sheet that differs from the present-day ice sheet. In contrast, assimilation methods use present-day observations to invert for the flow variables that cannot be measured, such as basal sliding or ice viscosity [*Arthern and Gudmundsson*, 2010], but therefore lack dependence on the ice sheet history. Furthermore, assimilation methods that do not account for the current climatic (and surface mass balance) trends can force the ice sheet model into a state that is far from equilibrium with the climate, and unnatural transients can emerge in prognostic modeling [*Seroussi et al*., 2011]. Both methods therefore have advantages and drawbacks, as discussed in this section, as the ideal starting configuration for projections of ice sheet evolution is an ice sheet that matches the present-day observations but that is also in imbalance due to past climatic changes.

[10] To illustrate the results of the various initialization processes, the observed ice sheet surface elevation of the ALBMAP v1 dataset [*Le Brocq et al*., 2010], shown in Figure 1, is compared in Figure 2 to the starting configuration for the SeaRISE experiments. The actual initial surface elevations are shown in the supporting information, Figure SM1. The models that initialize by assimilation methods (AIF and ISSM, shown in Figures 1a and 1b, respectively) are by nature a close match to the present-day configurations, since the procedure holds the ice sheet geometry (including the margin and grounding line positions) to that of the present day and tunes the internal fields to match target surface velocities. The target surface velocities are either balance velocities or observed velocities. Balance velocities are derived from the surface topography, ice thickness, and surface mass balance data [e.g., *Bamber et al*., 2000]. (The procedure assumes that the ice sheet is in steady state and that ice dynamics can be approximated by the shallow ice approximation, allowing integration of the ice flux from the ice divide to the margins [e.g., *Budd and Carter*, 1971; *Budd and Warner*, 1996]. The resulting balance velocities therefore represent depth and time averaged velocities [*Price et al*., 2011].) Observed velocities are obtained from multiple satellite interferometric synthetic-aperture radar (InSAR) scenes, acquired over a number of different time periods, and are therefore transient observations of an ice sheet that is in imbalance [*Price et al*., 2011]. Because of the large uncertainties in surface mass balance, ice thickness, and surface slope in coastal regions, balance velocities can be unreliable in marginal areas [*Bamber et al*., 2000; *Rignot et al*., 2011], but InSAR velocities are unavailable for parts of the ice sheet, in particular over ice divides where the low velocities

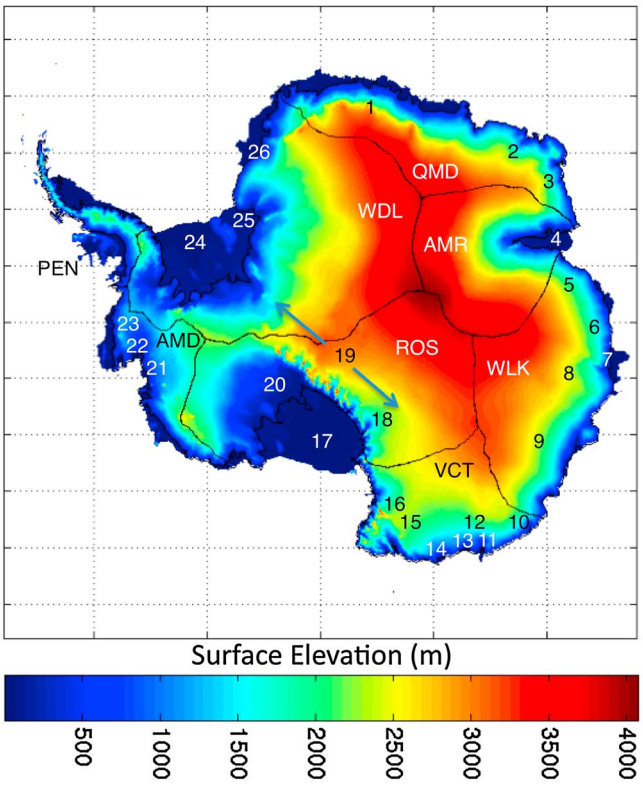

Figure 1. Observed surface elevation of modern-day Antarctica [*Le Brocq et al.*, 2010]. Drainage divides (black lines) are shown for the eight regions discussed in the text, along with the location of the geographical features mentioned in the text. Regions clockwise from the North: QMD, AMR, WLK, VCT, ROS, AMD, PEN, and WDL. Geographical features: 1, Dronning Maud; 2, Enderby; 3, Kemp; 4, Amery; 5, Princess Elizabeth; 6, Wilhem II; 7, Denman Glacier/ Shackleton Ice Shelf; 8, Queen Mary; 9, Wilkes; 10, Terre Adelie; 11, Mertz; 12, George V; 13, Ninnis; 14, Queen Mary; 15, Oates; 16, Victoria; 17, Ross.; 18, Byrd; 19, TransAntarctics; 20, Siple; 21, Thwaites; 22, Pine Island; 23, Ellswoth.; 24, Ronne; 25, Filchner; and 26, Stancombs-Wills.

are comparable to the measurement error. This choice between balance and InSAR velocities will affect the prognostic simulations. AIF iterates the governing equations keeping the observed geometry and present-day climate forcing (temperature and surface mass balance) fixed and tunes the enhancement factor (a parameter allowing anisotropic flow) to match the balance velocities (shown in Figure SM2). ISSM also keeps the geometry and surface temperature fixed to the present-day observations but infers the basal friction [*Morlighem et al.*, 2010; *Larour et al.*, 2012a] to best match the InSAR-derived surface velocities of *Rignot et al.* [2011] (shown in Figure SM2) via formal inverse methods [*MacAyeal*, 1989] and computes a thermomechanical steady state to ensure compatibility between temperature and velocities. For both models, large deviations from the observed surface elevations in Figure 2 are predominantly confined to the Transantarctic Mountains, where the noise is a result of multiple interpolations between the initial dataset, the model mesh, and the SeaRISE standard output grid (a fixed 10 km horizontal grid). The fixed 40 km horizontal grid of AIF also leads to noise in the periphery of the ice sheet, an effect that is less severe with ISSM due to its anisotropic mesh that allows for a 2–3 km resolution over the fast ice streams and a coarser resolution in the interior.

[11] Different methods for interglacial spin-up exist, and as a result, the initial configurations for PennState3D, Potsdam, SICOPOLIS, and UMISM differ from each other and from the observed present-day configuration (Figure 2). Due to large uncertainty in past climatic conditions, interglacial spin-up can result in present-day ice sheet geometry that is different from the present-day setting. A remedy is the development of spin-up procedures that tune the ice sheet surface to that of the observed configuration by holding the surface fixed to that of the observed state for some part of the spin-up. PennState3D spins up over the last 5 million years, with paleo-variations for the surface mass balance and temperature based on deep-sea-core $\delta^{18}O$ and earth orbital cycles [*Pollard and DeConto*, 2009]. During the spin-up procedure, the surface elevation, bed topography, and grounding line positions are free to evolve without any present-day constraints. The resulting ice shelves are in some places larger than the present day, for example, the Filchner-Ronne and Amery. PennState3D overestimates the surface elevation over mountain regions, such as the Transantarctic Mountains and in the Peninsula, and over regions of strong flow that feed the Filchner or Shackleton ice shelves for example. The spin-up used in the Potsdam model is a two-step procedure that initially seeks thermal equilibrium by letting the temperature evolve for 300 kyr keeping the geometry fixed to that of the present day. This initial step is followed by a 70 kyr geometric relaxation period that allows the ice sheet surface and grounding line to evolve. The relaxation period is forced by the present-day surface mass balance and temperatures [*Martin et al.*, 2011; *Winkelmann et al.*, 2011]. As in the PennState3D model, large positive deviations occur with the Potsdam model over mountain regions and areas of fast flow that feed ice shelves, in particular the Peninsula, the catchment basin of the Pine Island and Thwaites Glaciers, or the basins that drain into the Ronne-Filchner and Ross Ice Shelves. In contrast, the Potsdam model underestimates the ice thickness along the ice divides of the East Antarctic ice sheet. SICOPOLIS spin-up begins with the present-day ice sheet geometry and allows the ice surface and grounding line to evolve over 100 years under isothermal conditions at $-10^{\circ}C$ everywhere in order to avoid spurious noise in the computed velocity fields [*Calov*, 1994]. Once the initial relaxation run is computed, the ice sheet surface and grounding lines are fixed for the remainder of the 250 kyr spin-up. Between 250 to 125 kyr before present, the spin-up is a steady state run with surface temperatures set to that of the ice Vostok δD record at 125 kyr before present. The last step of the spin-up, from 125 kyr to present day, is a transient simulation with variable surface temperature derived from the Vostok δD record converted to temperature using the relation by *Petit et al.* [1999]. Due to the predominantly fixed-topography spin-up, SICOPOLIS's initial configuration is in close agreement with the present-day ice sheet. The thickness anomalies are generally less than 200 m, with increasing thickness deviations along the periphery of the ice sheet. The spin-up for the UMISM model used ice core proxy temperatures to drive a 30 kyr variable climate

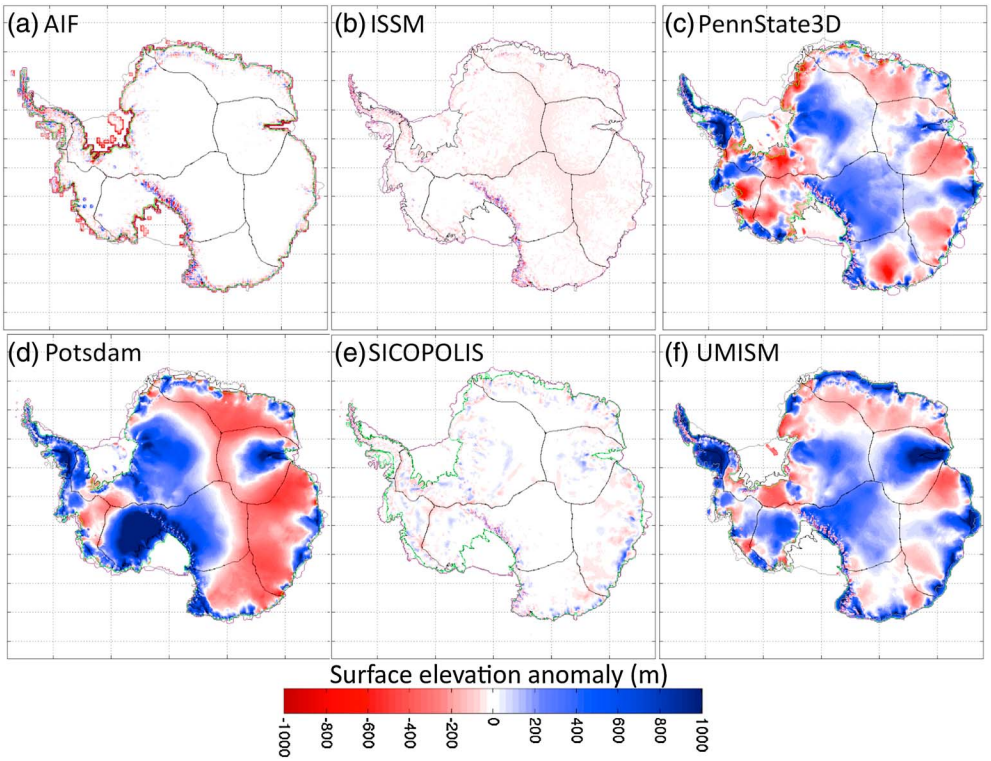

Figure 2. The anomaly in ice surface elevation at the start of the SeaRISE experiments: simulated minus modern-day Antarctica. Simulated grounding lines (green lines) and ice shelves extent (purple lines). Observed grounding lines (black lines) and ice shelves (gray lines) according to *Le Brocq et al*. [2010].

(surface mass balance and temperature) and does not involve any constraint or tuning for the ice sheet geometry. As a result, UMISM's grounding line is free to evolve during the spin-up, and the ice front position for most of the West Antarctic ice sheet lies further inland than the observed configuration. A more extensive glaciation results over the Peninsula and in some eastern regions such as Wilhelm II or Queen Mary Land. UMISM overestimates the ice thickness in the catchment basin that feeds the Amery and Shackleton ice shelves and, like PennState3D and Potsdam, the region inland from the Transantarctic Mountains.

[12] Other metrics could have been used to compare the initial state to the present day: observed surface velocities or ice volumes are commonly used. Initial ice velocities are included in the supporting information (Figure SM2) and provide a measure of how well the simulated ice sheet captures the distinct flow regimes in the ice sheet: from slow velocities in the interior of the ice sheet to faster flow over the ice streams and ice shelves. The ice model that assimilates the observed surface velocities, ISSM, reproduces as expected the observed large flow speeds that are concentrated over well-defined ice streams. The remaining models do also generally capture the large ice streams of the West Antarctic ice sheet, but the models that use the shallow ice approximation tend to produce surface velocities over the ice streams that are slower and more diffuse than currently observed.

[13] To assess the effect of the different initialization procedures on the prognostic simulation, models performed a control simulation by holding the climate constant to that of the end of spin-up condition for the models that carry out interglacial spin-up with varying climate or the present-day climate for models that obtain their starting configuration with data assimilation or fixed-topography spin-up methods. As the freely evolving topography spin-up contains a knowledge of the imbalance of the ice sheet due to past climatic forcing, as small change in volume is expected from the long-term background transient evolution [*Huybrechts and de Wolde*, 1999]. The volume above flotation (*VAF*), shown in Table 1, were obtained from post-processing of the SeaRISE experiments. The volume above flotation in ice volume equivalent VAF_{IE} is computed from $VAF_{IE} = A\ (H - Z\ (\rho_w / \rho_i))$ where A is the SeaRISE standard output grid cell area ($10\ \times 10$ km), H is the ice thickness, Z is the depth of the bedrock, and ρ_w and ρ_i are the densities of seawater and ice, respectively. The VAF_{IE} are then converted into global sea level equivalent (SLE) by assuming a constant oceanic surface area, A_{OC}, of 3.62×10^8 km^2 using $VAF = VAF_{IE}\ \rho_i\ /\ (A_{OC}\ \rho_w)$. Based on the data of *Le Brocq et al*. [2010], present-day *VAF* is 5529 cm SLE. The spin-up procedures used by PennState3D, Potsdam, and UMISM result in ice sheet geometries that differ by 4–7% from the current ice sheet (Figure 2 and Table 1) but experience a change in volume above flotation of order 1–2 cm SLE after 100 years of prognostic simulations (Table 1). In contrast, the initialization procedures of the AIF, ISSM, and SICOPOLIS models are within 0.05–0.4% of the observed ice sheet, but their control simulations grow by 9.31, 25.5, and 34.17 cm SLE, respectively, after 100 years, due to unnatural transients. The smaller drift resulting from the AIF model is predominantly due to the assimilation procedure that

Table 1. Initial Volume Above Flotation and Associated Change After 100 Years for the Control (CC_{100}–CC_0), Along With Sensitivity to SeaRISE Experiments ($Experiment_{100}$–CC_{100}) at 100 Years[a]

	AIF	ISSM	PennState3D	Potsdam	SICOPOLIS	UMISM	Mean
Initial (CC_0)	5532	5512	5752	5859	5521	5929	5684
CC_{100}–CC_0	9.31	25.55	2.00	−0.08	34.17	1.31	12.04
$C1_{100}$–CC_{100}	2.45	2.65	1.09	2.66	−3.26	−1.83	0.62
$C2_{100}$–CC_{100}	3.63	3.98	3.75	3.85	−2.40	−2.72	1.68
$C3_{100}$–CC_{100}	4.62	5.31	4.37	4.84	−2.54	−3.71	2.14
$S1_{100}$–CC_{100}	−18.09	−21.94	−7.59	−14.24	−27.70	−18.78	−18.06
$S2_{100}$–CC_{100}	−25.94	−31.83	−10.28	−19.51	−33.09	−17.74	−23.07
$S3_{100}$–CC_{100}	−33.43	−41.24	−12.87	−23.96	−44.40	−12.03	−27.99
$M1_{100}$–CC_{100}	−4.27	X	−12.25	−1.05	−7.88	−7.93	−6.68
$M2_{100}$–CC_{100}	−61.40	X	−84.11	−63.99	−31.46	−100.82	−68.35
$M3_{100}$–CC_{100}	−297.58	X	−119.10	−344.96	−57.30	−898.81	−343.55
$C1M1_{100}$–CC_{100}	−1.75	X	−9.46	1.6	−8.99	−9.88	−5.69
$C1S1_{100}$–CC_{100}	−15.64	−19.41	−5.73	−11.97	−25.33	−20.78	−16.47
$C1S1M2_{100}$–CC_{100}	−92.04	X	−92.42	−83.12	−93.90	−117.10	−95.71

[a]Subscripts refer to time. X indicates no submission from the model. Units are in centimeter sea-level equivalent (cm SLE).

accounts for the present-day surface mass balance in the computation of the surface balance velocities and that prescribes surface mass balance in the surface boundary conditions for the steady state assimilation. It is assumed that the initialization procedures affect the experiments and control simulation in a similar manner over the timescales considered, so that these unwanted unnatural adjustments can be removed by taking the difference between the experiment and control simulations. This assumption was tested in the early stage of SeaRISE with four simulations: two different control climate and a combination of control climate and amplified sliding forcing. Despite the use of different control climate, the two "experiment minus control" volume evolutions were nearly identical [e.g., *Greve et al*., 2011]. The approach of removing the control from the experiment implicitly assumes that the long-term background evolution does not feedback, nor influence, the behavior caused by the experiment. The consequence is that the natural transients due to the long-term background evolution are also removed, and therefore, any responses to our sensitivity experiments are in addition to these legacy changes.

3. SeaRISE Experiments

[14] SeaRISE explores the sensitivities of ice sheet models to climate-driven changes in boundary conditions at the upper and lower surfaces and perimeter. The imposed forcings are chosen to represent a warmer and wetter atmosphere, increased basal velocities, and warmer oceanic waters beneath floating ice shelves. The rational for these choices of sensitivity experiments is explained in *Bindschadler et al*. [2013] and is summarized in this section.

3.1. Atmospheric Experiments (C1, C2, and C3)

[15] The atmospheric forcing consists of anomalies in surface temperature and mass balance (i.e., precipitation minus ablation). These fields are derived from the ensemble mean of 18 models running the A1B scenario from the IPCC AR4 (T. Bracegirdle, personal communication, 2009). The A1B scenario represents rapid economic growth relying upon a balance of fossil and non-fossil fuel sources [*IPCC*, 2007]. Because the IPCC AR4 climate models made 100 year runs starting in calendar year 1998, and the SeaRISE simulations begin in 2004, we apply variable atmospheric forcing for the first 94 years of each experiment before holding this forcing constant at year 100 values. While the A1B scenario increases CO_2 emissions until roughly 2050 with a gradual decrease thereafter, more extreme emissions are certainly possible. We therefore consider A1B (our C1 experiment) along with scenarios in which the A1B temperature and mass balance anomalies are increased by 50% (C2) or doubled (C3). (We choose intensification of A1B over use of more extreme scenarios such as A1F1 or A2 to simplify the analysis by maintaining the same spatial and temporal patterns of change. The A1F1 temperatures by 2100 are about 50% greater than the A1B scenario and comparable to the temperatures for the RCP8.5 scenario considered by the IPCC AR5 [*Rogelj et al*., 2012].) The temporal patterns of the A1B temperature and precipitation anomalies, averaged over the Antarctic ice

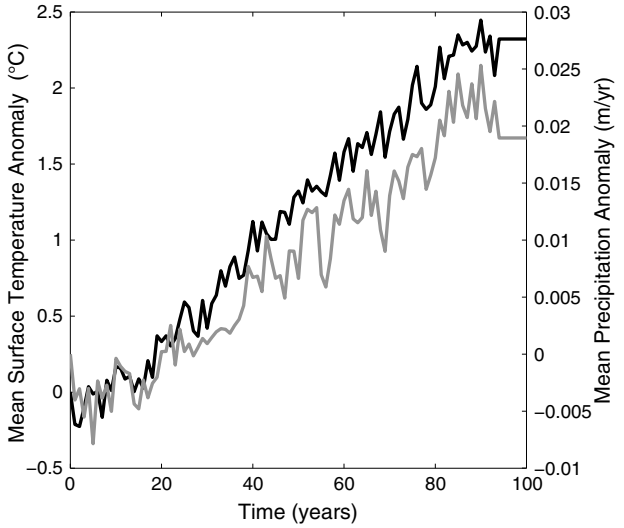

Figure 3. Surface temperature (black) and precipitation (gray) anomalies over the Antarctic ice sheet corresponding to the IPCC AR4 A1B scenario, which form the basis of the SeaRISE atmospheric scenarios.

sheet, are shown in Figure 3. The implementation of this forcing is somewhat model dependent, as models with various positive degree day (PDD) schemes calculated their own surface mass balance (thus allowing feedback between atmospheric forcing and the evolving ice-sheet surface elevation), while others directly applied the values given by the SeaRISE datasets.

3.2. Basal Sliding Experiments (S1, S2, and S3)

[16] The enhanced basal lubrication experiments are based upon the observed doubling of the flow speeds of Jakobshavn Isbrae in West Greenland and Helheim and Kangerdlugssuaq glaciers in South Greenland [*Joughin et al*., 2004, 2008a, 2008b; *Stearns and Hamilton*, 2007]. While this scenario is more likely in Greenland than in (non-peninsular) Antarctica, we apply this forcing to assess modeled interior ice-sheet response to acceleration of outlet glaciers and ice streams. We consider amplification of basal sliding by factors of 2, 2.5, and 3 (experiments S1, S2, and S3, respectively). Implementation of this forcing is model dependent, with those models that apply a basal velocity boundary condition able to directly multiply this velocity while those models that apply a basal stress boundary condition must appropriately modify their sliding coefficients.

3.3. Ice Shelf Melting Experiments (M1, M2, and M3)

[17] The effects of warming ocean waters beneath ice shelves (whether due to overall oceanic warming or to inshore advection of already-warm water masses) are considered in experiments that apply melt rates of 2, 20, and 200 m/yr (M1, M2, and M3, respectively). A melt rate of 2 m/yr would represent a roughly order of magnitude increase in average melting beneath the Ross and Filchner-Ronne ice shelves but is consistent with current observations near the fronts of both shelves, where tidal currents and a seasonally warmer upper ocean drive increased melting [*Holland et al*., 2003; *Joughin and Padman*, 2003; *Horgan et al*., 2011]. Increasing the melt rate to 20 m/yr corresponds roughly to the average melting reported by *Shepherd et al*. [2004] for ice shelves in the Amundsen Sea Embayment that are exposed to warm ($> 1°C$) Circumpolar Deep Water. Our highest melt rate, 200 m/yr, is not meant to represent a plausible ocean circulation scenario. Rather, this extreme melt rate is the simplest way of implementing the end-member case of sudden ice shelf removal (a phenomena that has been observed over the ice shelves in the Peninsula) while avoiding the numerical shocks that would result from this forcing being applied instantaneously to our models. Ocean circulation and ice shelf cavity shape play an important role in the location of melting at the ice-water interface [e.g., *Jenkins and Doake*, 1991]. However, melt rates are generally expected to be highest at or near the grounding line [*Williams et al*., 2001; *Payne et al*., 2007], and melting concentrated in this area has the greatest effect on grounding line retreat and thinning of interior ice [*Walker et al*., 2008; *Gagliardini et al*., 2010]. As with our other forcings, implementation is model dependent. The melt rates are either applied uniformly beneath all floating ice in those models that explicitly contain ice shelves or applied only beneath the grounding line in models that do not contain ice shelves (UMISM and AIF). The UMISM model does however approximately represent ice shelf dynamics through appropriate boundary conditions at the grounding line (backstress following *Thomas* [1973] and thinning rate according to *Weertman* [1974]). Grounding line retreat is implemented by a hydrostatic floating condition in most models, except for PennState3D, which applies in addition a parameterization based on *Schoof* [2007a], and ISSM, which did not participate in the experiment.

3.4. Combination Experiments (C1S1, C1M2, and C1S2M2)

[18] In a realistic warming scenario, it is likely that the ice sheet would be affected by multiple external forcings. While the assumption that the result would simply be the sum of the results due to each individual forcing may be attractive, the complexity of ice dynamics makes it questionable to expect a priori that the response will be linear over timescales of interest. We therefore carry out several combination experiments (C1S1, C1M2, and C1S2M2) that simultaneously apply two or three of our individual forcings.

4. Basin Sensitivity to SeaRISE Experiments

[19] The sensitivity of the Antarctic ice sheet to the SeaRISE forcings is first explored in Figures 4 and 5 via a regional analysis of the change in ice volume above flotation after 100 simulated years. The sensitivity at the continental scales is shown in Table 1. The regional analysis considers eight basins that were defined in Figure 1: (1) QMD: the basins of the East Antarctic ice sheet, which includes Queen Maud, Enderby, and Kemp Lands; (2) AMR: the catchment area of the Amery ice shelf; (3) WLK, which comprises Princess Elizabeth, Wilhelm II, Queen Mary, and Wilkes Lands; (4) VCT: the basins formed by Terre Adelie, George V, Oates, and Victoria Lands; (5) ROS: the basins feeding the Ross ice shelf; (6) AMD: the basins flowing into the Amundsen Sea; (7) PEN: the Peninsula; and (8) WDL: the basins flowing into the Ronne-Filchner Ice Shelf and the Weddell Sea. In each of these regions, the change in volume above flotation (ΔVAF) is calculated via the difference

$$\Delta VAF = VAF_{\mathrm{exp}} - VAF_{\mathrm{cc}}, \tag{1}$$

where the VAF values for the experiment and control, VAF_{exp} and VAF_{cc}, respectively, were obtained from post-processing of the SeaRISE submissions.

4.1. Basin Sensitivity to Atmospheric Forcings

[20] *Bindschadler et al*. [2013] describe the continent wide response of the Antarctic ice sheet to the SeaRISE experiments and point out that for the atmospheric forcing experiments (C1, C2, and C3), some models predict a gain in ice mass while others predict a mass loss at year 100. Figure 4 illustrates that these ΔVAF mass losses or gains are of order 0.1 to 5 cm SLE and small compared to the sliding or ocean melt experiments. Models that predict similar ice sheet wide mass changes (Table 1) can have regional differences. For example, the ice sheets simulated by the AIF and Potsdam models gained a comparable amount of mass in the C1 experiment and experienced a

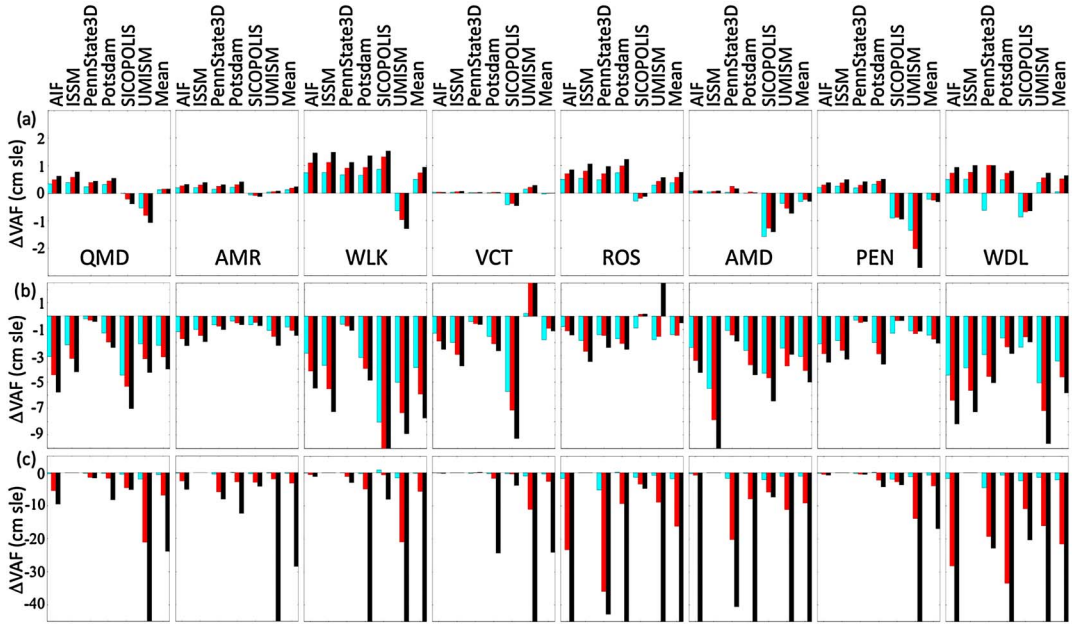

Figure 4. The change (experiment minus control) in the volume above flotation resulting from the suite of single forcings for eight regions of the Antarctic ice sheet after 100 simulated years. (a) Atmospheric forcings: ΔVAF_{C1} (blue), ΔVAF_{C2} (red), and ΔVAF_{C3} (black). (b) Basal sliding forcings: ΔVAF_{S1} (blue), ΔVAF_{S2} (red), and ΔVAF_{S3} (black). (c) Oceanic forcings: ΔVAF_{M1} (blue), ΔVAF_{M2} (red), and ΔVAF_{M3} (black).

growth comparable to PennState3D simulations for the C2 and C3 forcings, yet their regional ΔVAF are not all equal. Another example (with similar overall mass change but regional differences) is SICOPOLIS and UMISM in the C2 experiment. As with the overall response, responses of the individual models within each region may not even agree as to whether there is mass gained or lost. For example, in the QMD, AMD, and PEN regions, the ice sheets from the AIF, ISSM, PennState3D, and Potsdam models gained mass, while the ice sheets from the SICOPOLIS and UMISM models lost mass. With the exception of SICOPOLIS, all models experience an increase in *VAF* over the ROS region. Despite SICOPOLIS's predictions of mass loss in the above regions, it does not predict a loss everywhere; gain is predicted over the WLK basin that is comparable to AIF, ISSM, PennState3D, and Potsdam. Other mass gains that are consistent in their magnitude include AIF, ISSM, PennState3D, and Potsdam in the catchment basin of the Amery Ice Shelf (AMR) and the Ross Sea (ROS).

4.2. Basin Sensitivity to Basal Sliding Forcings

[21] For the sliding experiments, the AIF and UMISM models yield similar ice-sheet-wide mass loss to the S1 forcing (Table 1), but again, the individual regional responses differ. The mass losses from the UMISM model are larger than those of the AIF model in the WLK, ROS, and WDL basins but are smaller in the QMD and PEN basins. In the VCT basin, the AIF model simulates a mass loss, while the UMISM model projects a mass gain. Only the AMR and AMD regions experience a comparable ΔVAF with the UMISM and AIF models under the S1 forcing. Although ISSM and SICOPOLIS have a comparable ice sheet wide mass loss for the S2 forcing, the mass losses from the two models are never similar at the basin scale, with ISSM resulting in a greater mass loss compared to SICOPOLIS in all regions apart from the QMD, WLK, and ROS regions. Turning to the response to the S3 forcing, Antarctic-wide ΔVAF of similar magnitude arises from PennState3D and UMISM, but the regional analysis reveals an unexpected behavior: PennState3D and UMISM have the most distinct responses. PennState3D is generally one of the least responsive to the S3 forcing, and UMISM the most sensitive to this forcing, with large growth in the VCT and ROS regions that is mitigated by the decline over the remaining of the ice sheet. The end result is that both PennState3D and UMISM predict a similar modest mass loss.

4.3. Basin Sensitivity to Ice Shelf Melting Forcings

[22] The most sensitive regions to the melting suite of experiments are as expected the basins forming the West Antarctic ice sheet (ROS, AMD, and WDL), a region considered vulnerable to marine ice sheet instability [*Mercer*, 1978; *Weertman*, 1974] due to the large ice shelves that buttress the grounded ice sheet that rests below sea level [*Thomas*, 1979]. In contrast, the least sensitive region is the VCT basin that contains a handful of small ice shelves. The UMISM model is an exception in the VCT basin, due to an implementation of the forcings that erodes the grounded ice sheet, as we shall see in section 6. The M1 experiment can lead to a small growth of the grounded ice sheet, for example, in the AMR region with the PennState3D model or in the WLK basin with SICOPOLIS, whereas the other models suggest a negligible mass loss. These regions contain either a confined ice shelf (AMR region) or ice shelves that are small compared to the grid size in the control simulation (WLK region). This growth will be further explored in section 7. As seen in the atmospheric and basal sliding forcings, a mass loss that

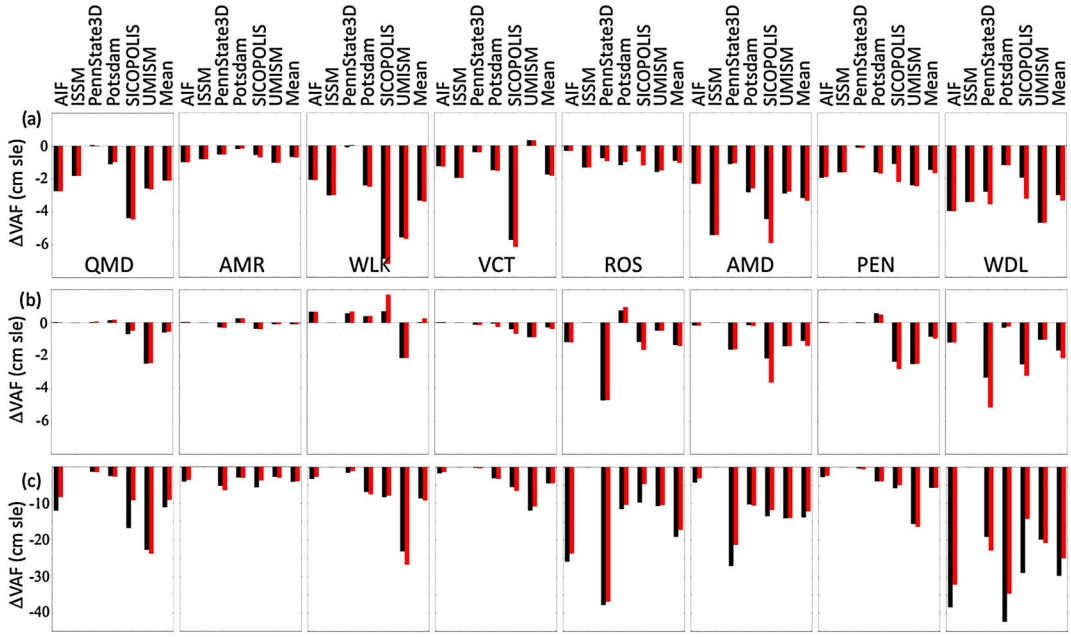

Figure 5. Comparison of the change in volume above flotation (experiment minus control) resulting from the suite of combination experiments to the sum of individual forcings for eight regions of the Antarctic ice sheet after 100 simulated years. (a) ΔVAF_{C1S1} (black) versus $\Delta VAF_{C1} + \Delta VAF_{S1}$ (red). (b) ΔVAF_{C1M1} (black) versus $\Delta VAF_{C1} + \Delta VAF_{M1}$ (red). (c) ΔVAF_{C1S1M2} (black) versus $\Delta VAF_{C1} + \Delta VAF_{S1} + \Delta VAF_{M2}$ (red).

is comparable at the continental scale can result in distinct basin sensitivities, as illustrated with the AIF and Potsdam models with the M1, M2, and M3 forcings (Table 1 and Figure 4c).

4.4. Basin Sensitivity to Amplified Forcing

[23] With all models, when the response to the C1 forcing leads to a mass gain, the effect of the C2 and C3 experiments is an amplified mass gain. When the C1 forcing results in a mass loss, however, the response to the amplified forcing differs. ISSM and PennState3D experience a reduced mass loss, UMISM an increased mass loss, while SICOPOLIS either gains or losses mass. The response to the amplified basal sliding forcings is more uniform: enhanced sliding results in a negative ΔVAF, except for UMISM and SICOPOLIS, which can both experience a growth in the ROS basin. The VCT basin also experiences a growth in the UMISM simulations. Amplifying the basal melt rate forcings also leads to an increase in mass loss in all basins.

4.5. Basin Sensitivity to Combination Forcings

[24] The combination experiments can be used to explore whether the ice sheet response to multiple forcings that are applied simultaneously is similar to the sum of the individual responses or whether they result in a stronger/weaker response indicating positive or negative feedbacks. Figure 5 compares the ΔVAF resulting from the combination forcing to the sum of the individual forcings, for all three combination experiments (C1S1, C1M1, and C1M1S2). These three combination experiments generally lead to a mass loss in all basins, except for the C1M1 forcing, which can result in a growth (Figure 5b). The WLK region is such an example, where most models indicate a mass gain. Looking at the responses to the individual C1 and M1 forcing (Figures 4a and 4c), the trend in the WLK region is to gain mass with the C1 forcing and to be relatively insensitive to the M1 forcing. The mass loss from the C1S1 forcing (Figure 5a) in the WLK region is less than the mass loss from the S1 forcing (Figure 4b), a behavior that is again explained by the tendency for mass gain with the C1 forcing. For most models and basins, summing the contributions of the individual forcings usually provides a reasonably accurate approximation of the response to the combination forcing. However, this approach does not always work and can preclude potential feedbacks, in particular when melt scenarios are considered (see section 8), and thus, reliable investigation of the response to multiple forcings does require the forcings to be simultaneously applied.

[25] The regional analysis presented in this section does not however elucidate whether the ΔVAF are caused by a change in ice thickness that is uniform throughout or localized within a region, or whether these responses are associated with a grounding line retreat resulting in an ice sheet that covers a smaller area, for example. To gain insight into the source of the regional ΔVAF necessitates an investigation of the spatial change in ice thickness. We now focus our analysis on the spatial patterns of thickness change for the C1, S1, M2, and the C1S1M2 sensitivity experiments.

5. Spatial Response to the Atmospheric C1 Experiment

[26] The spatial change in volume above flotation at a given year is explored by computing the difference in ice

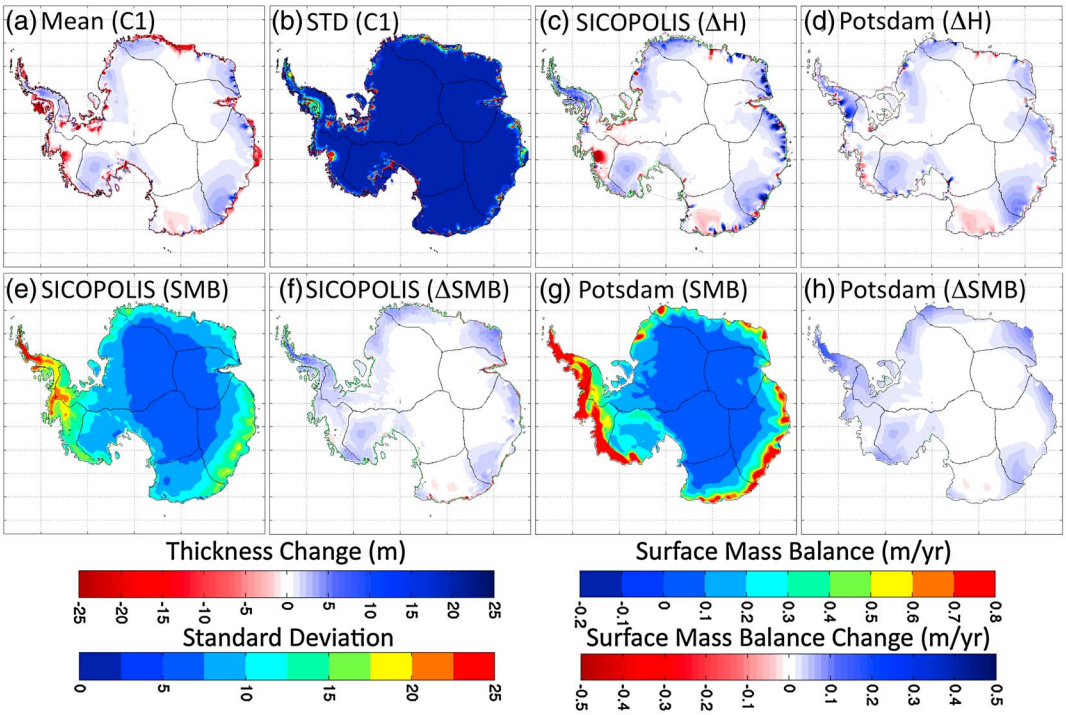

Figure 6. The ensemble mean thickness change from the (a) control and (b) standard deviation resulting from the C1 experiment after 100 simulated years, along with the thickness contribution from the most (c) negative (SICOPOLIS) and (d) positive (Potsdam) ΔVAF. (e, g) Surface mass balance and (f, h) surface mass balance anomaly for these models at 100 years. The corresponding figures for all models are shown in the supporting information (Figures SM3, SM4, and SM5). The grounding line for the C1 experiment at 0 and 100 years is shown in black and green, while ice shelf extent at 0 and 100 years are shown in gray and purple, respectively.

sheet thickness between an experiment and the control simulation for each model. The individual model responses (which are shown in the supporting information, Figure SM3) are then combined to form ensemble statistics: maps of the mean response and standard deviation. As the experiments might lead to a change in areal coverage of the ice sheet compared to the control run, the ensemble statistics are computed on any 10×10 km SeaRISE output grid that contains nonzero ice sheet thickness in either experiment or control simulation.

[27] The C1 experiment, which imposes the A1B anomalies in surface temperatures and precipitation without any amplification, is expected to result in a growth where surface mass balance anomalies are positive and a thinning over regions of negative surface mass balance. The ensemble mean thickness change, shown in Figure 6a, is characterized by a thinning over the margins of the ice sheet and a thickening over the steep coastal slopes. Exceptions to the coastal growth include George V Land in VCT, the region between the Dronning Maud Land and Enderby Land in the QMD, and the Amundsen Sea sector. Isolated large thinning occurs over regions of high flow, such as Byrd Glacier in the Transantarctic Mountains or in WDL over the Stancomb-Wills Glacier. Localized growth is seen in Kemp Land and Mertz and Ninnis Glaciers located in the QMD and VCT regions. The dominant pattern of thinning occurs throughout the basins that drain into the Amundsen Sea and over the Peninsula. These two regions resulted in the largest mass loss in Figure 4a, but the map illustrates that some growth does occur over many ice streams on the northeastern side of the Peninsula. Conversely, the regions experiencing the largest growth, namely, ROS and WLK, are two regions that experience a small interior growth over a large area, which more than compensates the peripheral thinning. The low standard deviation in Figure 6b indicates a consistency in individual model behavior over most of the ice sheet. High values of standard deviations are predominantly confined to the Peninsula and over isolated "hot spots" of fast flow, reflecting the spread in models' responses in these faster flowing regions.

[28] After 100 years of simulations, SICOPOLIS has lost more ice than the other models, while the Potsdam model produces the largest gain of mass (Table 1). Their respective changes in ice volume due to the C1 forcing compared to the control simulation (ΔVAF of -3.27 and 2.66 cm SLE) arise from distinct responses in ice sheet thicknesses, as illustrated in Figures 6c and 6d. Both models exhibit thinning along the grounding line of the Amery Ice Shelf, and the ensemble mean broad scale response over the steep coastal slopes, but with distinct spatial magnitudes and spatial extents. In particular, SICOPOLIS's response displays a high spatial variability over the periphery of the ice sheet that is often absent with the Potsdam model. For example, in QMD, SICOPOLIS's

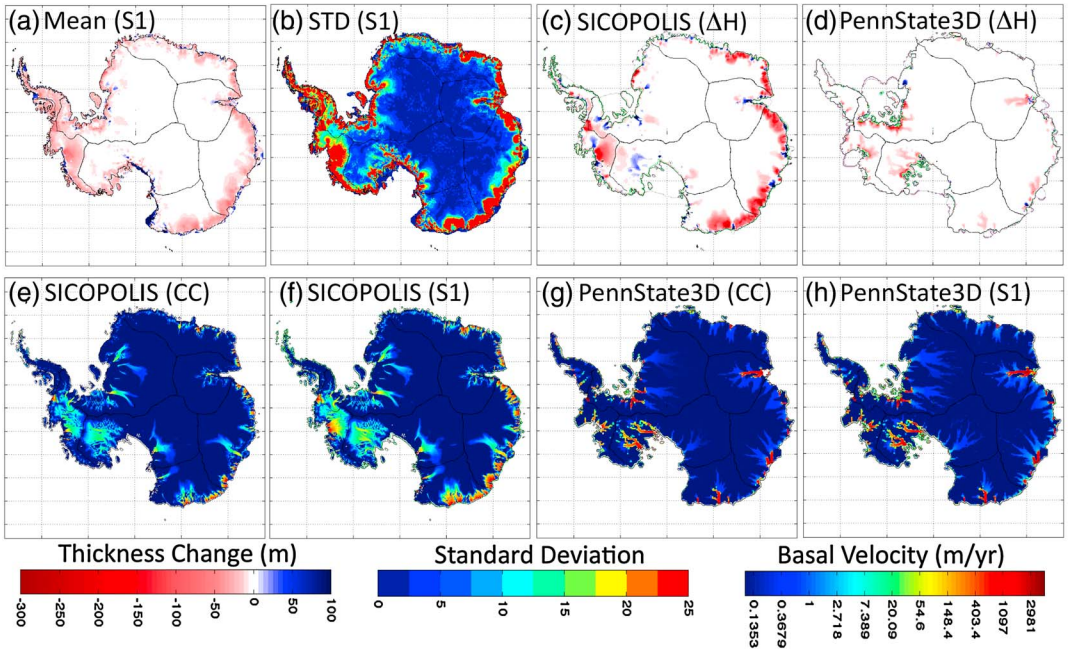

Figure 7. The ensemble mean thickness change from the (a) control and (b) standard deviation resulting from the S1 experiment after 100 simulated years, along with the thickness contribution from the (c) maximum (SICOPOLIS) and (d) minimum (PennState3D) models. The basal velocities from the control and S1 experiments for (e, f) SICOPOLIS and (g, h) PennState3D at 100 years. The corresponding figures for all models are shown in the supporting information (Figures SM6, SM7, and SM8). The grounding line for the S1 experiment at 0 and 100 years is shown in black and green, while ice shelf extent at 0 and 100 years are shown in gray and purple, respectively.

localized growth balances the localized thinning to result in a negligible ΔVAF (Figure 4a). SICOPOLIS's localized thinning over the grounding line of the Ronne-Filchner Ice Shelves (WDL) and over the Siple Coast (ROS) outweighs the interior growth. The largest mass loss of SICOPOLIS occurs in the Amundsen Sea sector and can be attributed to the large thinning over the Thwaites and Pine Island Glaciers in AMD that do not appear with the Potsdam model.

[29] The different responses from the Potsdam and SICOPOLIS models can be in part traced back to the surface mass balance (SMB) used by these two models. The surface forcings, shown in Figures 6e and 6g, differ between the two models for two reasons: distinct initial conditions and 100 year SMB anomalies. The Potsdam model applies an initial accumulation that is based on the data of *van de Berg et al*. [2006], while SICOPOLIS prescribes the accumulation of *Arthern et al*. [2006]. Both datasets have similar characteristics: high accumulation in coastal regions and low accumulation in the interior of the continent. Differences in the two datasets are mainly over the Peninsula, the western tip of Ellsworth Land (AMD), and along the Wilkes Land coast, where the accumulation from the data of *van de Berg et al*. [2006] is greater than that of *Arthern et al*. [2006]. The use of different initial SMBs should not dominate the ice sheet thickness change shown in Figures 6c and 6d, as these initial differences subtract out in the experiment minus control approach. The future precipitation and temperature anomalies are the same for both models, as they originate from the A1B climate model anomalies provided by SeaRISE, but the ablation is calculated in SICOPOLIS by a positive degree day (PDD) scheme that alters the surface mass balance. The Potsdam simulations do not use a PDD scheme and therefore prescribe the A1B anomalies directly. The average A1B surface temperature anomaly of 2.25°C results in higher precipitation (Figure 3) but negligible surface melting (Figure 6h). The SMB anomaly at 100 years for the SICOPOLIS model, displayed in Figure 6f, therefore differs due to the ablation over low elevation coastal regions such as the grounding lines. The pattern of thickness change resulting from the difference between experiment and control simulation is highly correlated to the 100 year SMB anomaly. SICOPOLIS's thinning over the Amery grounding line can indeed be largely attributed to the negative anomaly, even though the imposed SMB field is positive in this region.

[30] The ice shelves and grounding lines positions are little affected by these experiments in both models, a result consistent with the work of *Huybrechts and de Wolde* [1999], for warming below 5°C. However, the thickness change at 100 years also contains a response from past forcings. We attribute the thickness changes in Figures 6c and 6d that have no correlation with the 100 year anomaly to past surface mass balance anomaly. The thinning over Thwaites glacier that is seen in both models (albeit of different spatial extent and magnitude) is such an example of a response due to earlier negative surface mass balance in the Amundsen Sea Sector.

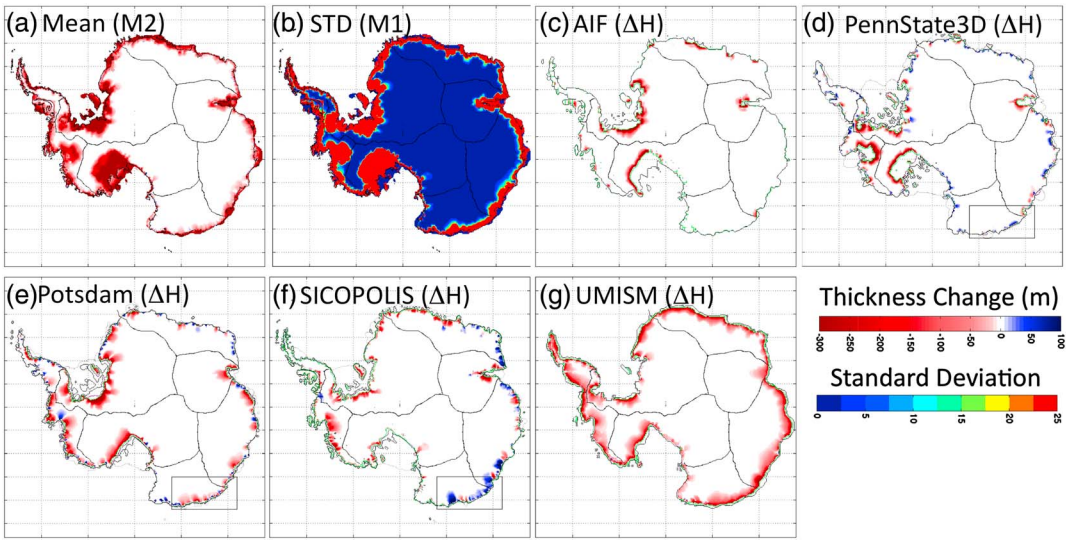

Figure 8. The ensemble mean thickness change from the (a) control and (b) standard deviation resulting from the M2 experiment at 100 years. The thickness change from the (c) AIF, (d) PennState3D, (f) Potsdam, (g) SICOPOLIS, and (h) UMISM models. Grounding lines at 0 and 100 years are shown in black and green lines, while ice shelf extent at 0 and 100 years are shown in gray and purple, respectively. Inset demarks the region in the VCT basin that is investigated in Figure 9.

6. Spatial Response to the Basal Sliding S1 Experiment

[31] The S1 experiment investigates the response of the ice sheet due to a step change that increases the basal velocities by a factor of 2 at the beginning of the simulation. This scenario is more applicable to the Greenland ice sheet but is undertaken to investigate the response to a speed up of the flow at the base of the grounded ice sheet. The suite of basal sliding experiments results in the most consistent model-to-model response, with an ice sheet wide mass loss for all models after 100 years in the simulations. The regional analysis in section 4 indicates a negative ΔVAF for most regions but also suggests that growth could occur. Increased basal sliding should initially lead to grounding line (or ice front margin) advance and thickening due to the increased ice flux. Upstream from the margins, a thinning over areas that have sped up and associated surface adjustments that propagate inland are anticipated due to the downstream change in ice flow and mass transfer. The ensemble behavior, shown in Figure 7a, is dominated by negligible change over the interior of the ice sheet, a thinning over the ice streams, and isolated thickening along the periphery of the ice sheet due to the coastal advance. In particular, the positive ΔVAF resulting from UMISM in the region that drains into the Ross Ice Shelf, and in the VCT region (Figures 4 and SM6), can now be attributed to peripheral growth downstream of the Transantarctic Mountains and along the coast of Oates Land, two regions that are mostly ice-free rock. The standard deviation for the ensemble is low throughout most of the deep interior, with the spread in model responses occurring over the ice streams, reflecting the large differences in modeled initial velocities over the fast ice streams.

[32] The two extreme responses for this experiment are from the SICOPOLIS and PennState3D models, with a ΔVAF in Table 1 of -27.7 and -7.59 cm SLE, respectively. In Figure 7c, SICOPOLIS's thinning occurs predominantly over the fast-flowing ice streams of the eastern periphery of the Antarctic ice sheet, Thwaites Glacier, and Stancomb-Wills Glacier. The maximum thinning occurs immediately upstream of the grounding line and reduces further inland. However, not every ice stream experiences a thinning: Pine Island Glacier and the ice streams feeding the Ross and the Ronne-Filchner Ice Shelves are examples. The response of PennState3D is different in its location and pattern: maximum thinning occurs at the terminus of the large ice streams of the Siple Coast, Thwaites, and Pine Island Glaciers, and the ice streams flowing into the Ronne-Filchner Ice Shelves. Furthermore, PennState3D's thinning does not extend as far inland as SICOPOLIS's. The Amery region also experiences thinning upstream of the grounding line with PennState3D, but the increase in ice discharge leads to a grounding line advance. This S1 upstream thinning and grounding line advance is also predicted on Thwaites by the higher-order flow band model PennState2D [*Parizek et al.*, 2013].

[33] For both models, the determination of areas that are experiencing basal sliding at the beginning of any simulation is a complex process that involves thermal and dynamical feedback in the spin-up procedure. In addition, as the ice sheet in experiment S1 evolves differently than that of the control simulation, different basal stresses and temperatures will emerge during the S1 and CC simulations, such that the ratio of experiment to control basal velocities will not remain constant in time. Nonetheless, further insight into the source of SICOPOLIS's and PennState3D's distinct

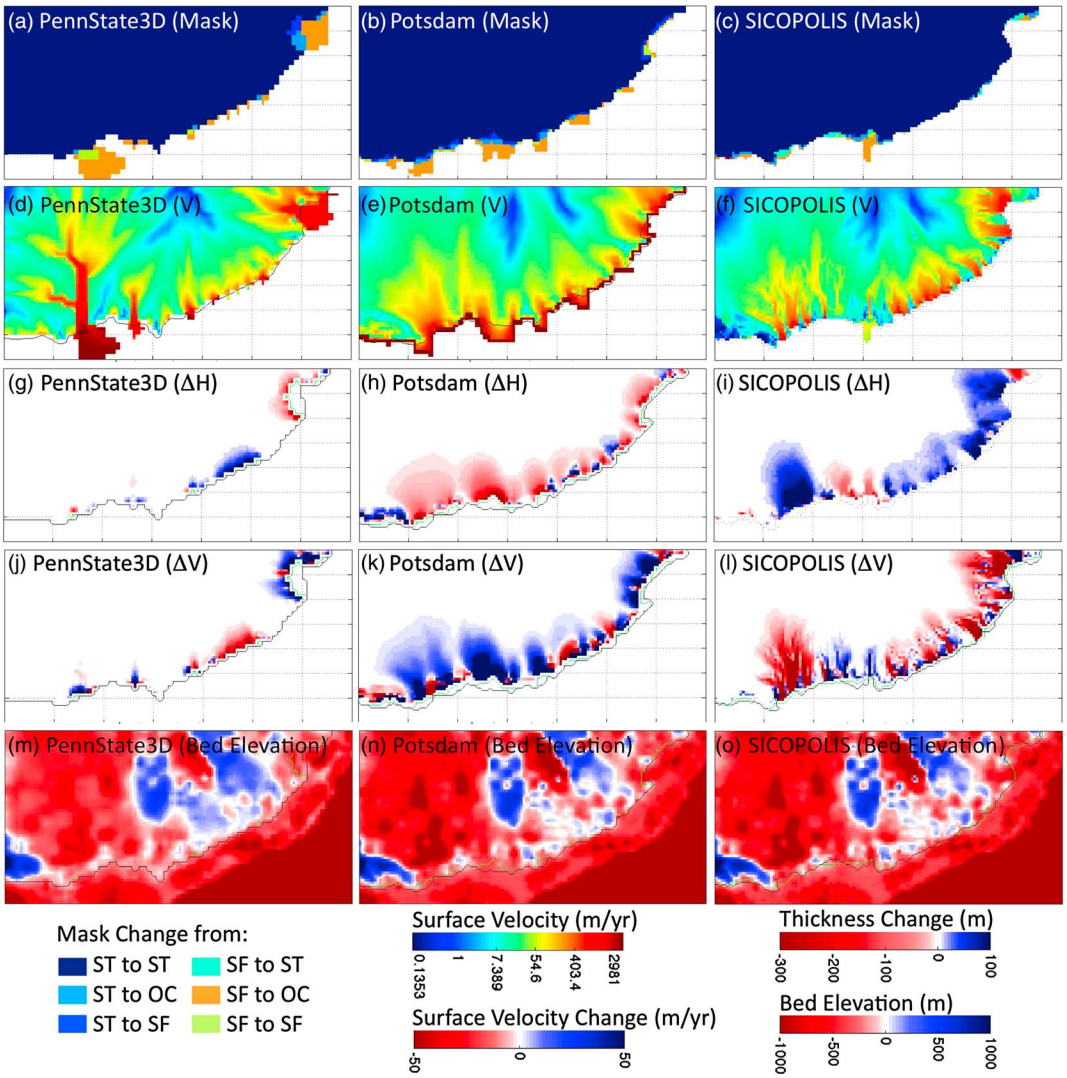

Figure 9. Change in mask classification at 100 years due to the M2 forcing compared to the initial mask (time 0) in the VCT basin for the (a–c) PennState3D, Potsdam, and SICOPOLIS models. Mask considered are ice sheet (ST), ice shelf (SF), and ice-free ocean (OC). "ST to OC" indicates that the pixel was initially a grounded ice sheet, which has become at 100 year an ice-free ocean pixel. (d–f) Initial surface velocities, (g–i) ice thickness change, and (j–l) surface velocity change resulting from the M2 experiment compared to the control at 100 years for the PennState3D, Potsdam, and SICOPOLIS models. (m–o) Initial bed and bathymetry for the PennState3D, Potsdam, and SICOPOLIS models.

responses is gained by looking at the basal velocities for the control and experiments (Figures 7e–7h). First, the spatial extent of the regions of fast flow is different in the control simulations: the bases of PennState3D's ice streams are long, narrow, well-defined channels. In contrast, SICOPOLIS's sliding occurs over most of the catchment area of the Siple Coast and the Amundsen Sea sector, for example. Second, the modeled location and number of ice streams around Antarctica differ. In VCT, for example, the tributaries of Cook, Ninnis, and Metz are the only regions of fast flow for PennState3D, whereas SICOPOLIS contains more ice streams in this region. Third, the magnitude of the basal velocities is generally larger at the ice stream onset and slower at the grounding lines, with SICOPOLIS compared to PennState3D.

[34] As a result, the applied forcings are not the same. The increased sliding of PennState3D is confined to regions that were already fast flowing. With SICOPOLIS, sliding intensifies over a larger area and further inland; the result is that many small ice streams merge and form faster and wider ice streams. With both models, thinning occurs in regions of increased flow, as long as high basal velocities occur at the grounding line of the ice stream. SICOPOLIS's low basal velocities in the vicinity of the grounding zone of the Amery Ice Shelf prevent the increased ice flux, due to enhanced flow upstream, from discharging into the ice shelf, and result in a thickening of the ice sheet upstream from the grounding line. The contrasting responses from the adjacent Pine Island and Thwaites Glaciers in SICOPOLIS (thickening versus

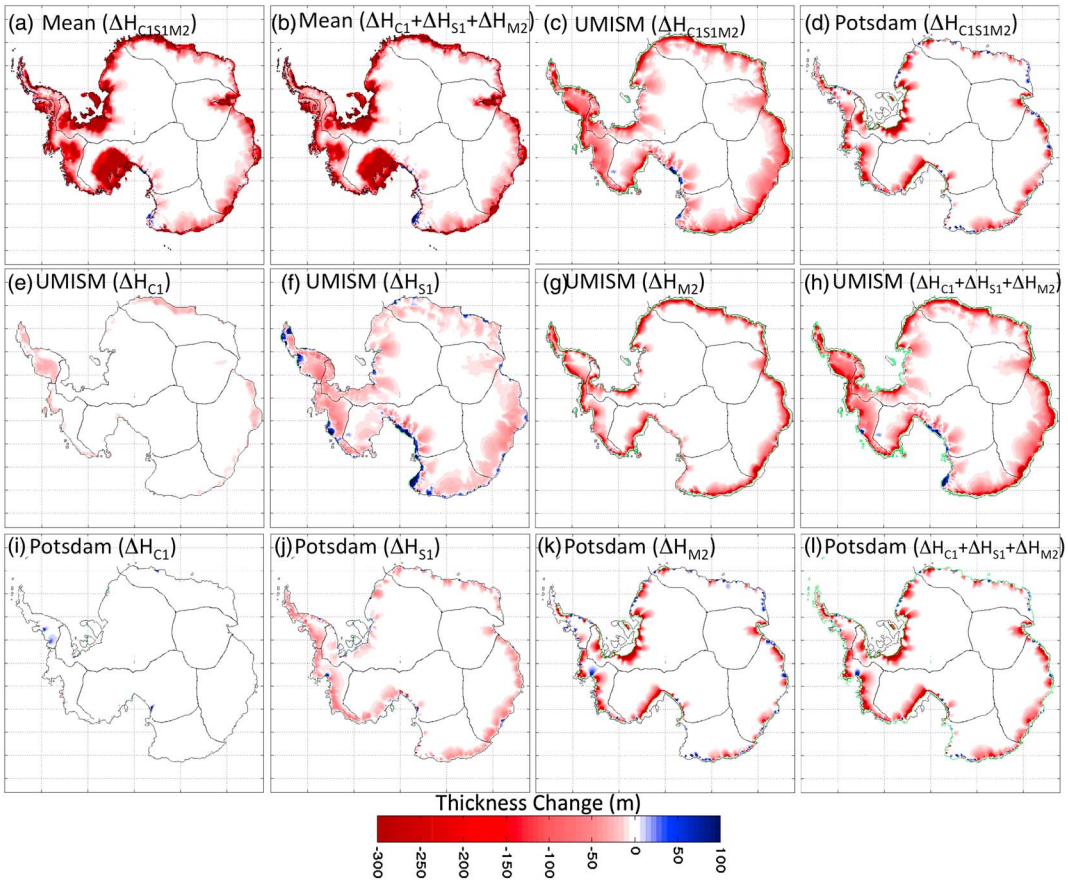

Figure 10. The ensemble mean thickness change from the control resulting from the (a) C1S1M2 experiment after 100 years, along with sum of the thickness change from the (b) C1, S1, and M2 experiments. The thickness contribution from the maximum (UMISM) and minimum (Potsdam) models for (c, d) the C1S1M2 forcing, (e, i) the C1 forcing, (f, j) the S1 forcing, (g, k) the M2 forcing, and (h, l) the sum of the C1, S1, M2 experiments. The corresponding figures for all models are shown in the supporting information (Figure SM9). The grounding line for the C1S1M2 experiment at 0 and 100 years is shown in black and green, respectively.

thinning) are again due to whether the increased ice flow can reach the grounding line, which is the case for Thwaites but not for Pine Island Glacier due to the bed being frozen in the control simulation upstream from the grounding line of Pine Island Glacier.

7. Spatial Response to the Ice Shelf Melting M2 Experiment

[35] The spatial response to the melting suite of experiments is illustrated with the M2 scenario, which imposes a spatially uniform melt rate of 20 m/year beneath all floating ice. The melting of confined ice shelves and associated loss in buttressing is expected to result in an increased inland ice discharge [*Sanderson*, 1979; *Thomas*, 1979] and a thinning of the grounded ice sheet upstream from the grounding line. The change in ice thickness and surface slope in the transition zone between ice sheet and ice shelf flow regimes results in an increase in driving stress and ice flux at the grounding line that can cause the grounding line to migrate. Depending on the bedrock configuration in the vicinity of the grounding line, a positive feedback can be established [*Weertman*, 1974; *Schoof*, 2007a, 2007b]. According to these 2-D theoretical studies, when the grounding line retreats into an inland-deepening bed, the increased ice thickness results in an increased grounding line mass flux and thus further retreat and potential instability of the marine ice sheet [e.g., *Mercer*, 1978]. The ensemble mean response (Figure 8a) features a thinning of the periphery of the ice sheet in regions where the ice meets the ocean. The thinning is largest over the ice streams that feed the large Ronne-Filchner and Ross Shelves, along with the Pine Island and Thwaites Glaciers. These regions have in common that their bedrock lie below sea level. The response in the Amundsen Sea Sector (AMD), with large thinning of the interior that lessens toward the coast, results from diversity in modeled responses. The standard deviation (Figure 8b) is larger in magnitude and extent compared to that of the C1 and S1 experiment, due to the diversity in model responses in each basin (Figure 4c). With this melt rate, the least sensitive model is SICOPOLIS (ΔVAF of −31.46 cm SLE), followed by Potsdam (ΔVAF of −63.99 cm SLE), AIF (ΔVAF of −61.4 cm

SLE), PennState3D (ΔVAF of −84.11 cm SLE), and UMISM (ΔVAF of −100.82 cm SLE). This order changes for the other melting scenarios, however, as indicated in Table 1. Insight into the response to the M2 experiment therefore requires an analysis of the thickness change for all models that participated in the experiment.

[36] The complex thickness change of the ensemble mean is due to a combination of factors. The first factor is the implementation of the experiment. UMISM and AIF do not include ice shelves (Figure 2), so the melt rate is applied beneath the grounding line. AIF restricts the melting to the grounding line of its ice streams, while UMISM imposes melting at every grid cell where the ice sheet shares a boundary with the ocean. The remaining models impose the melt rates uniformly beneath the ice shelves. The second factor is the grid size that varies between the models (Table A1), which is known to greatly affect the grounding line response of 2-D models [*Vieli and Payne*, 2005; *Durand et al*., 2009a; *Goldberg et al*., 2009; *Parizek et al*., 2010; *Pattyn et al*., 2012], and whether the ice sheet models can resolve the ice stream and transition zone, which has a length scale of one to many ice thickness [*Chugunov and Wilchinsky*, 1996; *Pattyn et al*., 2006; *Schoof*, 2007a; *Nowicki and Wingham*, 2008]. The third factor is the treatment of the grounding line migration: all models apply the flotation condition, but PennState3D also includes the Schoof ice flux parameterization [*Schoof*, 2007a, 2007b; *Pollard and DeConto*, 2009]. This mass flux constraint allows coarse grid ice sheet models to reproduce grounding line evolution that is consistent with 2-D theoretical work on marine ice sheets [*Weertman*, 1974; *Schoof*, 2007a; *Pattyn et al*., 2012]. The fourth factor is the different initial configurations of the ice sheet (including grounding line positions and thicknesses as seen in Figure 2, as well as ice shelf extent), so from the start, the ice sheets considered in some models are more sensitive to the prescribed forcings than others. The fifth factor is the approximation used for modeling the dynamics of ice flow and, in particular, the stress transfer between ice shelves and ice sheets. The change in flow regime is implemented in the PennState3D and Potsdam models via a transition zone with shelfy-stream dynamics, where the shallow shelf approximation is augmented by additional basal drag [*MacAyeal*, 1989]. In the SICOPOLIS model, however, ice dynamics is at present simply shallow ice approximation over grounded ice sheet [*Hutter*, 1983; *Morland*, 1984] and shallow shelf approximation for floating ice [*Morland*, 1987]. The UMISM model approximately includes the effect of ice shelf stresses on the grounded ice sheet flow by imposing at the grounding line an ice shelf spreading rate [*Weertman*, 1957, 1974] and ice shelf back stress [*Thomas*, 1979].

[37] Together, these factors affect the grounding line evolution in each model, resulting in a grounding line retreat that is not homogeneous, as illustrated in Figures 8c–8g, and which dominates the ΔVAF shown in Figure 4c. The high and spatially uniform melt rate of 20 m/yr results in the rapid disintegration of the Antarctic ice shelves and complete removal of small ice shelves in East Antarctica. The grounding line of the PennState3D model retreats farther inland into the deep basins of the West Antarctic ice sheet than any other model, resulting in the largest ΔVAF for these regions. The M2 forcing does not lead to a complete removal of the Amery ice shelf, due to its confined configuration in a narrow embayment, and the increased ice discharge from the Lambert glacier. Because of its implementation of the forcing, UMISM erodes a vast portion of its periphery, making it the largest contributor of ice loss. The comparable ΔVAF for the QMD and WLK regions, resulting from the UMISM simulation, is due to a coastline of similar extent for these two regions. Where the melting is prescribed over the same grounding lines, both AIF and UMISM respond in a similar fashion to the models that have ice shelves: the grounding line retreats and inland thinning occurs.

[38] The negligible ΔVAF over the VCT basin is due to either no forcing being applied (AIF) or growth balancing the thinning for the PennState3D, Potsdam, and SICOPOLIS models (Figure 9). The growth in the PennState3D and Potsdam simulations occurs over small ice streams that used to drain into small ice shelves at the beginning of the simulation (Figures 9a and 9b). The M2 forcing results in a removal of the ice shelves in the early stage of the simulation and can lead to grounding line retreat. The bedrock in the vicinity of the initial grounding line switches from being below sea level downstream of the grounding line to being above sea level upstream of the grounding line. A retreat or thinning of the grounding line thus leads to a decrease in grounding line mass flux that in turn results in a thickening upstream from the grounding line. The thickening associated with the SICOPOLIS model also occurs over small diffuse ice streams that either terminated in the ocean or formed small ice shelves at the beginning of the simulation. After 100 years of simulations, the ice shelves are now grounded, and the switch from ice shelves to grounded ice sheet dynamics slows down the upstream inland flow. In the control simulation (not shown), these small ice shelves have also grounded and form a larger grounded ice sheet than with the M2 forcing, so the thickening is associated with allowing the ice sheet surface to freely evolve after the fixed-topography spin-up.

8. Spatial Response to the Combination C1S1M2 Experiment

[39] The spatial response for the combination experiments after 100 years is illustrated with the C1S1M2 forcing, which imposes simultaneously the A1B climate anomalies (C1), a sliding amplification by a factor of two (S1), and a melt rate of 20 m/year under floating ice (M2). The regional analysis presented in section 4 suggested that the ΔVAF from individual forcings was a reasonable first-order approximation to the response from simultaneous forcing, a result that also applies for the ice sheet volume temporal evolution at the continental scale [*Bindschadler et al*., 2013]. In this section, we show that these conclusions can be extended to the patterns of thickness change. The ensemble mean thickness change to the C1S1M2 forcing, shown in Figure 10a, is characterized by a thinning and grounding line retreat of the ice streams feeding the ice shelves. This thinning can extend

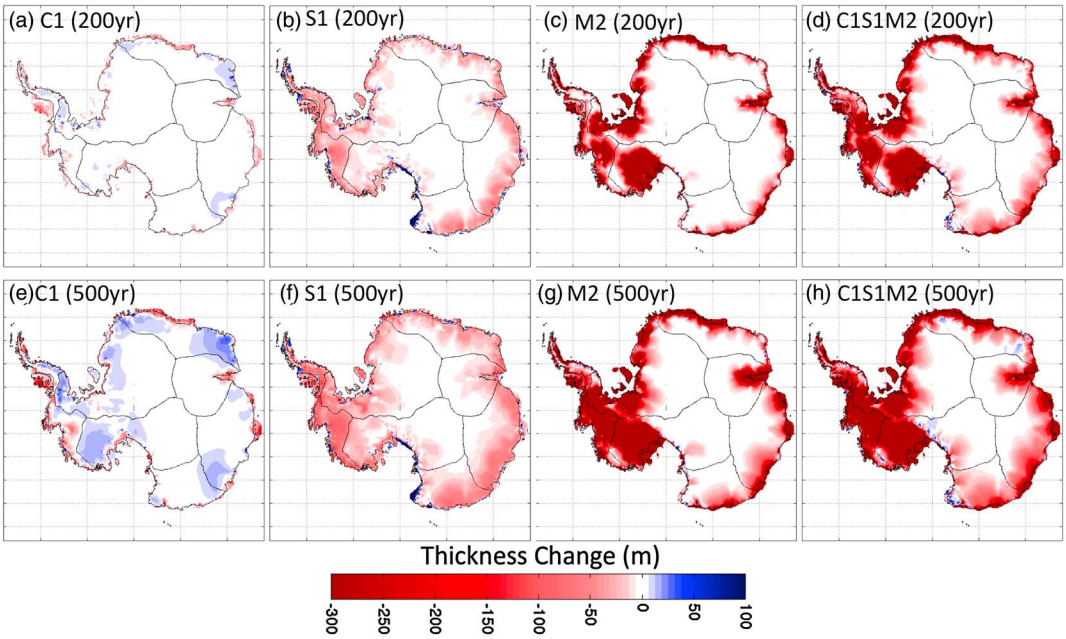

Figure 11. The ensemble mean thickness change from the control at 200 and 500 years resulting from (a, e) the C1 experiment, (b, f) the S1 forcing, (c, g) the M2 experiment, and (d, h) the C1S1M2 forcing. The corresponding figures for all models are shown in the supporting information (Figures SM10–SM17).

into the interior of some catchment areas. The thickness change from the sum of the individual forcings, displayed in Figure 10b, captures the spatial characteristic of the thickness response to the C1S1M2, although with smaller magnitudes. Differences are concentrated at the ice sheet margins, as illustrated for example in the southwestern tip of the VCT basin, where the thickness change from the sum of the individual forcings predict a thickening that is not always present in the C1S1M2 forcing.

[40] As the ensemble mean has the tendency to smooth the signals from the individual models, we demonstrate that for the most and least sensitive models, the thickness change associated with the simultaneous forcing is also captured by combining the responses from the individual forcings. UMISM was the most sensitive model in the M2 experiment and is also the most responsive to the C1S1M2 experiment (Table 1). The ΔVAF from this combination experiment is −117.10 cm SLE, compared to −1.83, −18.78, and −100.82 cm SLE for the C1, S1, and M2 forcings, respectively. The model that leads to the smallest ΔVAF (−83.12 cm SLE) with C1S1M2 is Potsdam, which experienced a growth of 2.66 cm SLE with C1, and mass losses of −14.24 cm SLE with S1 and −63.99 cm SLE with M2. For both models, the patterns of thickness change due to the C1S1M2 (Figures 10c and 10d) and sum of individual responses (Figures 10h and 10l) do indeed correlate in both spatial extent and magnitude. The implication is that the complex response to the C1S1M2 forcing can be decomposed and attributed to the relevant C1, S1, or M2 forcings.

[41] At each location, the thickness response of the combination experiment resembles that of the dominant basal melting forcing, with the pattern of thickness change either amplified or attenuated depending on the relative magnitude of the other two sliding and climate forcings. For example, in the UMISM simulations the melting of the peripheral ice in the C1S1M2 experiment (Figure 10c or 10h) leads to a grounding line retreat that is comparable to the M2 response (Figure 10g). The associated thinning upstream from the grounding line with the M2 forcing, however, propagates further inland to reach regions that were sensitive to the S1 forcing (Figure 10f), as demonstrated for example with the Amery Ice Shelf. Regions that were little affected by the M2 forcing in the UMISM simulation become vulnerable with the combination experiment, as illustrated by the glaciers flowing through the Transantarctic Mountains that experience a thinning with C1S1M2 that is characteristic of the S1 forcing. With the Potsdam simulations, the S1 thinning (Figure 10j) dominates over the responses of the M2 and C1 experiments (Figures 10k and 10i) in the PEN and WLK regions, for example. In contrast, the thinning patterns of the tributaries of the Amery Ice Shelf or the Siple Coast are characteristic of the M2 experiment. The different grounding line responses in the WDL region (Figure 10l), however, illustrate that the response to the C1S1M2 experiment can differ from the superposition of the individual forcings. This is due to feedbacks and grounding line migration that arise from the simultaneous forcings that are not captured by the summing approach.

9. Discussion and Conclusions

[42] SeaRISE investigated the sensitivity of the current generation of ice sheet models to external forcings that altered in turn the atmospheric conditions, the basal sliding beneath the grounded ice sheet, and the basal melting under floating ice, as well as different

combinations of these three factors. Differences in modeled response of the Greenland [*Nowicki et al*., 2013] and Antarctic ice sheets to similar SeaRISE forcings highlight the glaciological significance of their unique environmental and geographic settings. The ensemble mean ice sheet wide ΔVAF is distinct for these forcings: the Antarctic ice sheet grows with the warmer atmospheric conditions (cf. shrinking of the Greenland ice sheet, where surface ablation and runoff already account for ~50% of its annual mass loss) [*Huybrechts and de Wolde*, 1999; *Church et al*., 2001], while it loses mass with the dynamic forcings (as does Greenland, but with regional signatures indicative of the much smaller embayments, the far less pervasive marine instability in which a collapse of the ice sheet results from the positive feedback associated from the grounding line retreat into deeper water and the higher accumulation rates that limit the inland extent of thermally activated sliding). The magnitude of volume change is correlated with the applied forcing and increases with the amplified experiments. The Antarctic Ice Sheet volume change from the three increased sliding experiments (−18.84, −24.09, and −29.10 cm SLE) falls within the range of the two smallest oceanic melting forcings (−7.06 and −63.59 cm SLE), implying that intermediate melt rates would have resulted in a volume change that is comparable to the sliding experiments.

[43] The regional analysis of the ΔVAF after 100 years for the Antarctic Ice Sheet revealed that distinct regional responses emerge from the four types of sensitivity experiments, despite the diversity in individual model sensitivity. For example, the mean ΔVAF for the WLK basin suggests that this region gains the most mass as a result of the atmospheric (C1, C2, C3, and C1M1) forcing but that it also leads to the greatest mass loss in the suite of sliding experiments (S1, S2, S3, and C1S1). The most sensitive response and mass loss from the experiments C1, C2, and C3 occur over the basins flowing into the Amundsen Sea and the Peninsula, while it is the basins flowing into the Ronne-Filchner Ice Shelves that lead to the largest decline in *VAF* from the oceanic (M1, M2, M3, C1M1, and C1S1M2) experiments. The regional ΔVAF analysis therefore demonstrates that Antarctica is not affected by the forcings in a uniform manner: each basin has its own behavior. Some basins are more sensitive to changes in atmospheric conditions, while others mainly respond to oceanic or basal forcings. Insight into the non-uniform basin sensitivity is achieved from the spatial analysis of the ice thickness change for each of the applied forcings. The West Antarctic basins, with a bed below sea level, that drain into large ice shelves experience a substantial grounding line retreat compared to the East Antarctic basins that have a bed above sea level and drain into small ice shelves. For the atmospheric forcings, basin sensitivity is a function of regional setting. Basins grow with warming, except within low-latitude regions, where marginal thinning outpace inland thickening. For the increased sliding forcings, basin sensitivity is a function of flow regime, with basins dominated by high driving stress being more vulnerable than basins with low-surface-slope streaming ice.

[44] The spatial analysis demonstrates that the thickness change displays different characteristics (fingerprints or signatures) for each type of experiment. The atmospheric forcing results in a thinning that is concentrated at the grounding line of the ice sheet and a growth over the steep coastal slopes. The thickness change after 100 years is highly correlated with the pattern of surface mass balance anomaly. This suite of experiments results in the most uniform response from the models, as indicated by the low standard deviations. The 100 years timescale is too short to assess the evolving dynamical impact of the atmospheric forcing, which becomes apparent over longer time-scales. Note, for example that after 200 years and 500 years (Figures 11a and 11e), the thinning over Thwaites is amplified and the thinning over the grounding line of the Amery Ice Shelf has propagated inland. The dominant response, namely, the interior growth due to the accumulation, is still highly correlated with the surface mass balance anomaly. This behavior is expected given the very slow flow of most inland ice and therefore the relatively slow surface adjustments.

[45] The thickness change resulting from the increased basal sliding forcing is characterized by a thinning over the regions of fast flow due to the increased ice discharge. The thinning decreases toward the interior but propagates inland with time (Figures 11b and 11f), such that after 500 years, the interior of the ice sheet also lowers. The model-to-model differences are predominantly due to the spatial distribution, coverage, and magnitude of the basal velocities. The basal conditions beneath the ice mass are presently poorly known yet have controlling effect on ice flow [e.g., *van der Veen and Payne*, 2004; *Gudmundsson and Raymond*, 2008; *Heimbach and Bugnion*, 2009; *Stone et al*., 2010; *Larour et al*., 2012b]. Models have to infer important properties such as basal rheology and bathymetry, as well as the spatial distributions of both the resistance to basal sliding and the frozen/sliding regions. In addition, it is questionable whether ice stream dynamics can fully be captured by the coarse grids often used by the current ice sheet models, which will affect the determination of the basal friction in the initialization procedure. This forcing is more suitable to the Greenland ice sheet but illustrates that reducing the spread in models' responses, and hence uncertainty, requires an improved determination of the basal conditions from remotely sensed observations and field campaigns.

[46] The oceanic forcing leads to a shelf thinning (and in some cases ice shelf removal), causing a grounding line retreat and associated draw-down upstream of the grounding line. The thinning is initially concentrated in the coastal regions (Figure 8a) but with time clearly propagates inland (Figure 11g). However, after 500 years of simulations, the thinning does not extend as far inland as the thinning driven by the increased sliding forcing. The oceanic suite of experiments results in the most diverse response due to the differing implementations of the forcing (melting beneath the ice shelf versus beneath the grounding line) and treatments of the grounding line migration. In locations where models with and without ice shelves apply the oceanic forcing, such as the grounding lines of the Ross and Ronne-Filchner ice shelves, the response is not that distinct between the models if grounding line migration is simply based on the flotation condition. PennState3D imposes two conditions: hydrostatic equilibrium and grounding line flux condition based on *Schoof* [2007a], which according to theoretical work in 2-D [*Weertman*, 1974; *Schoof*, 2007b] provides the most robust grounding line evolution in coarse ice sheet models [*Pattyn et al*., 2012]. The two conditions allow the grounding line

of the PennState3D model to retreat into the deep interior of the West Antarctic ice sheet. In contrast, the models that prescribe a grounding line migration based on only the flotation condition do not retreat as far inland. However, real ice sheets flow in 3-D, and recent work in this parameter space, suggests that 2-D and 3-D marine ice sheets behave in different ways and could be less susceptible of instability [*Gudmundsson et al*., 2012]. Grid size is known to affect the behavior of grounding lines and can result in numerical artifacts [e.g., *Vieli and Payne*, 2005; *Gladstone et al*., 2012; *Pattyn et al*., 2012], motivating the recent development of continental ice sheet models with adaptive meshes in the vicinity of the grounding line [e.g., *Larour et al*., 2012a; *Martin et al*., 2011; *Seddik et al*., 2012; *Cornford et al*., 2013]. Grounding line migration thus continues to be a challenge for ice sheet models, and it is hoped that intercomparison exercises that focus on grounding line migration, such as MISMIP and MISMIP3d [*Pattyn et al*., 2012; *Pattyn et al*., 2013], in conjunction with theoretical and numerical studies on the physics of grounding lines [e.g., *Chugunov and Wilchinsky*, 1996; *Schoof*, 2007a,2007b, 2011; *Nowicki and Wingham*, 2008; *Alley et al*., 2007; *Durand et al*., 2009b; *Goldberg et al*., 2009; *Gladstone et al*., 2010; *Parizek and Walker*, 2010; *Katz and Worster*, 2010] and field campaigns such as *Mayer and Huybrechts* [1999], *Anandakrishnan et al*. [2003, 2007], or *Peters et al*. [2005] will reduce the spread in modeled responses. The forecast of grounding line evolution also requires a detailed knowledge of the bedrock topography [e.g., *Vieli and Nick*, 2011; *Durand et al*., 2011; *Parizek et al*., 2013], which can only be resolved by intensive surveys of the grounding zones of the Antarctic ice sheet.

[47] The simultaneous application of atmospheric, oceanic, and increased sliding forcings leads to a response that is a mixture of the signatures from the individual experiment. The peripheral thinning due to the oceanic forcing can now reach interior regions that were sensitive to the enhanced sliding experiment (Figures 10, 11d, and 11h). In the interior, the increased accumulation outweighs the surface draw-down from the enhanced basal slipperiness, so the thickness increases with time. On the time scales considered in this study, the sum of the responses to the individual forcings captures the spatial signature of the response to the simultaneous forcings, indicating that this first-order approximation is a valid estimator of the simultaneous response. The summing approach allows the identification of the source of the thickness change (ocean, atmosphere, or sliding) and could therefore become a new tool for the understanding of the observed complex response of the present-day ice sheet.

[48] The un-weighted ensemble analysis of the changes in ice thickness resulting from the SeaRISE forcings provides valuable information and insight into the spread in ice sheet volume evolution (hence sea level projections) presented in *Bindschadler et al*. [2013]. The un-weighted ensemble mean is the best estimate of the available model sample [*Weigel et al*., 2010] and, together with the standard deviation of the sample, highlights where models agree and disagree [*Gates et al*., 1999; *Knutti et al*., 2010b]. However, there is no guarantee that the ensemble trend is more likely or accurate than any single realization [e.g., *Giorgi*, 2005]. Understanding the source of the diversity in the model results is therefore crucial in order to reduce the uncertainty in the projection. Just as in any future climate simulation, the analysis presented here demonstrates that the model spread in the SeaRISE effort is due to a number of factors. The first factor is the problem of obtaining an initial configuration for the projection. The two commonly used methods, interglacial spin-up or data assimilation, have both advantages and drawbacks and will affect the determination of fields that cannot be measured (such as basal slipperiness). The second factor is the uncertainty in actual observations, which includes but is not limited to surface mass balance, basal topography, ice thickness, and surface velocities. An additional issue with these observations is that they can be transient quantities which are not measured at the same time, but ice sheet models require them to be simultaneous. The third factor is the uncertainty in the models' physics and discretization, as well as the implementation of the external forcing. The impact of the latter is too often underestimated. Both are limited by our understanding (or lack of understanding) of crucial processes that often occur at subgrid scale relative to the resolution used by continental ice sheet models and thus require parameterization. Grounding line migration is such an example. The fourth factor is the determination of the future forcing scenarios. Unfortunately, as demonstrated in this analysis, all ice sheet models face these limitations to some degree, so that it is extremely difficult to identify a set of models and projections that should be trusted in preference to others. One model might be more suitable for assessing the impact of a warmer atmosphere because of its initialization procedure, but its deficiencies in capturing grounding line migration, for example, might make its projections for oceanic forcing or combination experiments unreliable. Furthermore, it is not clear that a model with complex ice dynamic that assumes a Newtonian viscous bed is for projection purposes better than a simpler ice dynamic model that uses a more realistic representation of basal sliding. More work is thus required to evaluate individual ice sheet models' skills for projection, but this crucial and challenging task is left for future studies, as despite numerous studies, a reliable, robust method that assesses the projection skill of climate models has yet to be identified [*Knutti et al*., 2010a]. This type of studies is urgently needed for ice sheet models, and to facilitate these efforts, the output from each model participating in SeaRISE will be made publicly available. Despite the current uncertainties and the spread in model results, general trends that are consistent in all models do emerge from the SeaRISE forcings, and characteristic responses to the different types of sensitivity experiment are seen in both individual model and in the multi-model ensemble. The results presented here can therefore be viewed as a baseline for future ensemble forecast for the Antarctic ice sheet over the coming centuries and will allow the assessment of progress in sea-level forecasting skills from ice sheet models.

Appendix A: Model Descriptions

[49] This appendix summarizes in Table A1 the essential features of the ice models taking part in the Antarctic SeaRISE suite of experiments, along with the implementation of the forcings. The models often have additional capabilities that are not used in the SeaRISE experiments and therefore not included in Table A1.

Table A1. Characteristics of Antarctic Models Used in SeaRISE

Model	AIF	ISSM	PennState3D
Numerical method	Finite difference, Eulerian	Finite element; Arbitrary Lagrangian Eulerian (ALE)	Finite difference, Eulerian
Grid (horizontal; vertical)	H: 40 km average grid spacing V: 20 evenly spaced layers	H: Anisotropic (between 3 km on fast ice streams and 15 km in the interior) V: 14 layers non uniformly spaced	H: 20 km V: 10 unequal layers
Time step	1 year	2 months	0.5 to 1 year
Spin-up/Initialization	Iteration on the governing equations with the present-day ice sheet geometry and climate forcing. The balance velocity is used as the target to tune the stress configuration through an adjustable enhancement factor	Data assimilation to match present-day InSAR velocities and self-consistent temperature field	Last 5 million years spin-up with paleo-variations for the surface mass balance and temperatures
Ice flow mechanics	Higher order with longitudinal and vertical shear stresses	Higher order (Blatter-Pattyn)	Shallow Ice + Shelfy-Stream (hybrid)
Surface mass balance and temperature	SeaRISE-provided mean annual temperature. Positive degree day (PDD) method using SeaRISE suggested parameters	SeaRISE datasets as no PDD scheme	Positive degree day using SeaRISE modern mean annual air temperature and precipitation datasets, including a sinusoidal seasonal cycle, lapse rate corrections. (paleo spin-up variations based on deep-sea-core $\delta^{18}O$ and orbit)
Basal sliding	Weertman sliding law (m = 3). Experiment amplifies the sliding coefficient	Linear viscous sliding law. Experiment reduces the sliding coefficient.	Weertman sliding law with basal temperature dependence, experiment amplifies the sliding coefficient
Basal hydrology	None	None	None
Ice shelves	No. Melting rate for the experiments is applied to the perimeter grid points with a bed below sea level and limited to the grounding line of large ice shelves	Yes. No participation in melting experiment	Yes. Melt rates for experiment applied uniformly under the ice shelves
Grounding line (GL) advance/retreat	Ice sheet margin moves freely. Grounding line detected by the floatation condition	Fixed calving front and GL	GL is determined by a floating criterion. Uses *Schoof* [2007a, 2007b] parameterization of ice flux across grounding line versus thickness as an internal boundary condition. Calving based on divergence of large-scale flow
References	*Wang et al*. [2012]	*Morlighem et al*. [2010], *Seroussi et al*. [2011], and *Larour et al*. [2012a, 2012b]	*Pollard and DeConto* [2009, 2012]
Model	Potsdam	SICOPOLIS Antarctica	UMISM
Numerical method	Finite difference, Eulerian	Finite difference, Eulerian	Finite element quadrilaterals
Grid (horizontal; vertical)	H: 15 km V: 81 levels, non-uniformly spaced	H: 10 km V: 91 layers (terrain-following)	H: 10 km V:40 layers, non-uniformly spaced
Time step	Adaptive	Thickness, velocity: 0.01–0.02 year Temperature: 0.1–0.2 year	1 year
Spin-up/Initialization	300 ka fixed present-day ice geometry enthalpy equilibration, followed by a 70 ka transient run with present-day climate forcing (the first 20 ka thereof with ocean temperatures reduced by 0.05K). Present-day surface climate from RACMO [*Van de Berg et al*., 2006] and ocean temperatures and salinity from BRIOS [e.g., *Timmermann et al*., 2002]	First 125 ka steady state and then 125 ka transient (from the Eemian through the last glacial period until present), with fixed, slightly smoothed present-day topography	30,000 year, driven by ice core temperature proxy
Ice flow mechanics	Shallow Ice + Shelfy-Stream (hybrid)		Shallow ice

Table A1. (continued)

Model	AIF	ISSM	PennState3D
		Shallow ice for grounded ice. Shallow shelf for floating ice	
Surface mass balance and temperature	SeaRISE dataset as no PDD scheme	Present-day mean annual and mean summer surface temperatures by *Fortuin and Oerlemans* [1990]. Present-day accumulation by *Arthern et al.* [2006]. PDD by *Reeh* [1991] with factors of 8 mm/(d*K) for ice melt and 3 mm/(d*K) for snow melt	Mean annual temperature (MAT) from latitudinal and elevation lapse rates [*Fausto et al*., 2009] PDD with lat-dependent amplitude around MAT
Basal sliding	Nearly plastic power law [*Schoof and Hindmarsh*, 2010]. Experiment reduces the basal friction coefficient	Weertman sliding law with basal temperature dependence (p = 3, q = 2). Experiment amplifies the sliding coefficient	Non-linear Weertman sliding law; lubrication factor proportional to basal water amount. Experiment amplifies the lubrication factor
Basal hydrology	Basal melt water controls bed strength	Water content computed in near-basal temperate ice (max. 1%), basal melting rate computed under grounded ice	Basal water conserved; source calculated from basal melting
Ice shelves	Yes. Melt rates for experiment applied uniformly under the ice shelves	Yes. Melting rate for experiment applied uniformly beneath the ice shelves	No, but effect of ice shelf approximated by imposing at the grounding line *Weertman's* [1974] thinning rate and *Thomas*' [1973] backstress. Melting experiment applies melt rates at last grounded grid point
Grounding line (GL) advance/retreat	Ice shelf calving front migration based on kinematic first-order calving law [*Levermann et al.*, 2012]. Grounding line migration based on the flotation condition	Freely evolving ice margin based on the flotation condition, but limited to the present-day extent	Grounding limit shifts to position where surface falls below flotation height
References	*Winkelmann et al*. [2011] and *Martin et al.* [2011]	*Greve et al*. [2011] and *Sato and Greve* [2012]	*Fastook* [1993]

[50] **Acknowledgments.** A project of this magnitude and scope required extensive support from many persons not listed as authors. Data sets, both published and in pre-publication forms, were contributed by A. LeBrocq, H. Pritchard, B. Csatho (dh/dt), T. Bracegirdle, CReSIS, and NASA's IceBridge mission and posted on the University of Montana CISM web site to be available to all SeaRISE modelers. This web site also served as a discussion forum for SeaRISE during its early stages of model initialization and experiment design. The Los Alamos National Laboratory also offered use of a web site that became the repository of all communication files (telecom notes and meeting presentations of SeaRISE). Participation in SeaRISE remained voluntary and, in most cases, came without financial support. Thus, participants had to leverage off of existing funding activities with objectives that overlapped with SeaRISE goals.

[51] R. Greve, H. Seddik, and T. Sato were supported by a Grant-in-Aid for Scientific Research A (22244058) from the Japan Society for the Promotion of Science (JSPS). U. Herzfeld was supported by a NASA Cryospheric Sciences Award (NNX11AP39G). M. A. Martin was supported by the German Federal Ministry of Education and Research (BMBF). B. Parizek was supported by the U.S. National Science Foundation under grants 0531211, 0758274, 0909335, and the Center for Remote Sensing of Ice Sheets (CReSIS) 0424589 and by NASA under grants NNX-09-AV94G and NNX-10-AI04G. D. Pollard was supported by the US National Science Foundation under grants ANT-0424589, 1043018, 25-0550-0001, and OCE-1202632. S. F. Price and W. H. Lipscomb were supported by the U.S. Department of Energy (DOE) Office of Science Office of Biological and Environmental Research. Simulations were conducted at The National Energy Research Scientific Computing Center (supported by DOE's Office of Science under contract DE-AC02-05CH11231) using time awarded through DOE's ASCR Leadership Computing Challenge allocation to the project "Projections of Ice Sheet Evolution Using Advanced Ice and Ocean Models." Model development and simulations were also conducted at the Oak Ridge Leadership Computing Facility at the Oak Ridge National Laboratory, supported by DOE's Office of Science under contract DE-AC05-00OR22725. CISM development and simulations relied on additional support by K. J. Evans, P. H. Worley, and J. A. Nichols (all of Oak Ridge National Laboratory) and by A.G. Salinger (Sandia National Laboratories). H. Seroussi and M. Morlighem are supported by the NASA Cryospheric Sciences Program and Modeling Analysis and Prediction Program and a contract with the Jet Propulsion Laboratory Research Technology and Development Program. H. Seroussi was also supported by an appointment to the NASA Postdoctoral Program at the Jet Propulsion Laboratory, administered by Oak Ridge Associated Universities through a contract with NASA. Resources supporting this work were provided by the NASA High-End Computing (HEC) Program through the NASA Advanced Supercomputing (NAS) Division at Ames Research Center. E. Larour and E. Rignot further enabled their participation on SeaRISE. R. Walker was supported by NSF through grants 0909335 and CReSIS 0424589, by NASA under grants NNX-09-AV94G and NNX-10-AI04G, and by the Gary Comer Science and Education Foundation. W. Wang was supported by the NASA Cryospheric Science program (grant 281945.02.53.02.19). Finally, S. Nowicki and R. Bindschadler wish to gratefully acknowledge the unwavering encouragement and financial support from the NASA Cryospheric Science program for the core funding enabling SeaRISE to reach a successful conclusion. We thank the reviewers (two anonymous and A. Vieli), the Associate Editor P. Christoffersen, and the Editor B. Hubbard for their very thoughtful comments to the original draft that led to a more constructive final manuscript.

References

Alley, R. B., and I. Joughin (2012), Modeling ice-sheet flow, *Science*, *336*, 551–2, doi:10.1126/science.1220530.

Alley, R. B., S. Anandakrishnan, T. K. Dupont, B. R. Parizek, and D. Pollard (2007), Effect of sedimentation on ice-sheet grounding-line stability, *Science*, *315*, 1838–1841.

Anandakrishnan, S., D. E. Voigt, R. B. Alley, and M. A. King (2003), Ice stream D flow speed is strongly modulated by the tide beneath the Ross Ice Shelf, *Geophys. Res. Lett.*, *30*(7), 1361, doi:10.1029/2002GL016329.

Anandakrishnan, S., G. A. Catania, R. B. Alley, and H. J. Horgan (2007), Discovery of till deposition at the grounding line of Whillans Ice Stream, *Science*, *322*, 1835–1838.

Arthern, R. J., and G. H. Gudmundsson (2010), Initialization of ice-sheet forecasts viewed as an inverse Robin problem, *J. Glaciol.*, *56*, 527–533.

Arthern, R. J., D. P. Winebrenner, and D. G. Vaughan (2006), Antarctic snow accumulation mapped using polarization of 4.3-cm wavelength microwave emission, *J. Geophys. Res.*, *111*, D06107, doi:10.1029/2004JD005667.

Bamber, J. L., R. J. Hardy, and I. J. Joughin (2000), An analysis of balance velocities over the Greenland ice sheet and comparison with synthetic aperture radar interferometry, *J. Glaciol.*, *46*, 67–74.

van de Berg, W. J., M. R. van den Broeke, and E. van Meijgaard (2006), Reassessment of the Antarctic surface mass balance using calibrated output of a regional atmospheric climate model, *J. Geophys. Res.*, *111*, D11104, doi:10.1029/2005JD006495.

Bindschadler, R., et al. (2013), Ice-sheet model sensitivities to environmental forcing and their use in projecting future sea level (The SeaRISE Project), *J. Glaciol.*, *50*, 195–224, doi:10.3189/2013JoG12J125.

Budd, W. F., and D. B. Carter (1971), An analysis of the relation between the surface and bedrock profiles of icecaps, *J. Glaciol.*, *10*, 197–209.

Budd, W. F., and R. C. Warner (1996), A computer scheme for rapid calculations of balance-flux distributions, *Ann. Glaciol.*, *23*, 21–27.

Bueler, E., and J. Brown (2009), The shallow shelf approximation as a "sliding law" in a thermomechanically coupled ice sheet model, *J. Geophys. Res.*, *114*, F03008, doi:10.1029/2008JF001179.

Calov, R. (1994), Das thermomechanische Verhalten des Gronländischen Eisschildes unter der Wirkung verschiedener Klimaszenarien—Antworten eines theoretisch-numerischen Modells, (PhD Thesis, Technische Hochschule, Darmstadt).

Chugunov, V. A., and A. V. Wilchinsky (1996), Modelling of a marine glacier and ice-sheet-ice-shelf transition zone based on asymptotic analysis, *Ann. Glaciol.*, *23*, 59–67.

Church, J. A., J. M. Gregory, P. Huybrechts, M. Kuhn, K. Lambeck, M. T. Nhuan, Q. Qin, and P. L. Woodworth (2001), Changes in sea level, in *Climate Change 2001: The Scientific Basis: Contribution of Working Group I to the Third Assessment Report of the International Panel on Climate Change*, edited by J. T. Houghton et al., 881 pp., Cambridge Univ. Press, New York.

Cook, A., A. Fox, D. Vaughan, and J. Ferrigno (2005), Retreating glacier fronts on the Antarctic Peninsula over the past half-century, *Science*, *308*, 541–544.

Cornford, S. L., D. F. Martin, D. T. Graves, D. F. Ranken, A. M. LeBrocq, R. M. Gladstone, A. J. Payne, E. G. Ng, and W. H. Lipscomb (2013), Adaptive mesh, finite volume modeling of marine ice sheets, *J. Comput. Phys.*, *232*(1), 529–549, doi:10.1016/j.jcp.2012.08.037.

Durand, G., T. Zwinger, E. Le Meur, and R. C. A. Hindmarsh (2009a), Full Stokes modeling of marine ice sheets: Influence of the grid size, *Ann. Glaciol.*, *50*(2), 109–114.

Durand, G., O. Gagliardini, B. de Fleurian, T. Zwinger, and E. Le Meur (2009b), Marine ice-sheet dynamics: Hysteresis and neutral equilibrium, *J. Geophys. Res.*, *114*, F03009, doi:10.1029/2008JF001170.

Durand, G., O. Gagliardini, L. Favier, T. Zwinger, and E. le Meur (2011), Impact of bedrock description on modeling ice sheet dynamics, *Geophys. Res. Lett.*, *38*, L20501, doi:10.1029/2011GL048892.

Fastook, J. L. (1990), A map-plane finite-element program for ice sheet reconstruction: A steady-state calibration with Antarctica and a reconstruction of the Laurentide Ice Sheet for 18,000 BP, in *Computer Assisted Analysis and Modeling on the IBM 3090*, edited by H. U. Brown, IBM Scientific and Technical Computing Dept., White Plains, N.Y.

Fastook, J. L. (1993), The finite-element method for solving conservation equations in glaciology, *Comput. Sci. Engr.*, *1*, 55–67.

Fastook, J. L., and T. J. Hughes (1990), Changing ice loads on the earth's surface during the last glacial cycle, in *Glacial Isostasy, Sea-Level and Mantle Rheology, Series C: Mathematical and Physical Sciences, Vol. 334*, edited by R. Sabadini, K. Lambeck, and E. Boschi, Kluwer Academic Publishers, Dordrecht/Boston/London, 165–207.

Fastook, J. L., and M. Prentice (1994), A finite-element model of Antarctica: Sensitivity test for meteorological mass balance relationship, *J. Glaciol.*, *40*, 167–175.

Fausto, R. S., A. P. Ahlstrøm, D. Van As, C. E. Bøggild, and S. J. Johnsen (2009), A new present-day temperature parameterization for Greenland, *J. Glaciol.*, *55*(189), 95–105, doi:10.3189/002214309788608985.

Fortuin, J. P. F., and J. Oerlemans (1990), Parameterization of the annual surface temperature and mass balance of Antarctica, *Ann. Glaciol.*, *14*, 78–84.

Fox Maule, C., M. E. Purucker, N. Olsen, and K. Mosegaard (2005), Heat flux anomalies in Antarctica revealed by satellite magnetic data, *Science*, *309*, 464–467, doi:10.1126/science.1106888.

Gagliardini, O., G. Durand, T. Zwinger, R. C. A. Hindmarsh, and E. Le Meur (2010), Coupling of ice-shelf melting and buttressing is a key process in ice-sheet dynamics, *Geophys. Res. Lett.*, *37*, L14501, doi:10.1029/2010GL043334.

Gates, W. L., et al. (1999), An overview of the results of the Atmospheric Model Intercomparison Project (AMIP I), *Bull. Am. Meteorol. Soc.*, *80*, 29–55.

Giorgi, F. (2005), Interdecadal variability of regional climate change: Implications for the development of regional climate change scenarios, *J. Meteorol. Atmos. Phys.*, *89*, 1–15.

Gladstone, R. M., A. J. Payne, and S. L. Cornford (2010), Parameterizing the grounding line in flow-line ice sheet models, *Cryosphere*, *4*, 605–619, doi:10.5194/tc-4-605-2010.

Gladstone, R. M., A. J. Payne, and S. L. Cornford (2012), Resolution requirements for grounding-line modelling: Sensitivity to basal drag and

ice-shelf buttressing, *Ann. Glaciol.*, *53*, 97–105, doi:10.3189/2012AoG60A148.

Gleckler, P. J., K. E. Taylor, and C. Doutriaux (2008), Performance metrics for climate models, *J. Geophys. Res.*, *113*, D06104, doi:10.1029/2007JD008972.

Goldberg, D., D. M. Holland, and C. Schoof (2009), Grounding line movement and ice shelf buttressing in marine ice sheets, *J. Geophys. Res.*, *114*, F04026, doi:10.1029/2008JF001227.

Greve, R. (1997), A continuum-mechanical formulation for shallow polythermal ice sheets, *Phil. Trans. Royal Soc., Series A*, *355*, 921–974.

Greve, R., F. Saito, and A. Abe-Ouchi (2011), Initial results of the SeaRISE numerical experiments with the models SICOPOLIS and IcIES for the Greenland ice sheet, *Ann. Glaciol.*, *52*(58), 23–30, doi:10.3189/172756411797252068.

Gudmundsson, G. H., and M. Raymond (2008), On the limit to resolution and information on basal properties obtainable from surface data on ice streams, *Cryosphere*, *2*(2), 413–445.

Gudmundsson, G. H., J. Krug, G. Durand, L. Favier, and O. Gagliardini (2012), The stability of grounding lines on retrograde slopes, *Cryosphere*, *6*, 1497–1505, doi:10.5194/tc-6-1497-2012.

Heimbach, P., and V. Bugnion (2009), Greenland ice sheet volume sensitivity to basal, surface and initial conditions derived from an adjoint model, *Ann. Glaciol.*, *50*(52), 67–80.

Holland, D. M., S. S. Jacobs, and A. Jenkins (2003), Modelling the ocean circulation beneath the Ross Ice Shelf, *Antarct. Sci.*, *15*(1), 13–23.

Horgan, H. J., R. T. Walker, S. Anandakrishnan, and R. B. Alley (2011), Surface elevation changes at the front of the Ross Ice Shelf: Implications for basal melting, *J. Geophys. Res.*, *116*, C02005, doi:10.1029/2010JC006192.

Hutter, K. (1983), *Theoretical Glaciology: Material Science of Ice and the Mechanics of Glaciers and Ice Sheets*, p. 510, D. Reidel, Dordrecht.

Huybrechts, P. (1994), The present evolution of the Greenland ice sheet: An assessment by modelling, *Global Planet. Change*, *9*, 39–51, doi:10.1016/0921-8181(94)90006-X.

Huybrechts, P., and J. de Wolde (1999), The dynamic response of the Greenland and Antarctic ice sheets to multiple-century warming, *J. Climate*, *21*, 2169–2188.

IPCC (2007), *Climate Change 2007: The Physical Sciences Basis, Contribution of Working Group I to the Fourth Assessment Report of the Intergovernmental Panel on Climate Change*, edited by S. Solomon, et al., p. 996, Cambridge Univ. Press, New York.

Jenkins, A., and C. Doake (1991), Ice-ocean interaction on Ronne Ice Shelf, Antarctica, *J. Geophys. Res.*, *96*(C1), doi:10.1029/90JC01952.

Joughin, I., and L. Padman (2003), Melting and freezing beneath Filchner-Ronne Ice Shelf, Antarctica, *Geophys. Res. Lett.*, *30*(9), 1477, doi:10.1029/2003GL016941.

Joughin, I., W. Abdalati, and M. Fahnestock (2004), Large fluctuations in speed on Greenland's Jakobshavn Isbræ glacier, *Nature*, *432*, 608–610, doi:10.1038/nature03130.

Joughin, I., S. B. Das, M. A. King, B. E. Smith, I. M. Howat, and T. Moon (2008a), Seasonal speedup along the western flank of the Greenland Ice Sheet, *Science*, *320*(5877), 781–783.

Joughin, I., I. Howat, R. B. Alley, G. Ekstrom, M. Fahnestock, T. Moon, M. Nettles, M. Truffer, and V. C. Tsai (2008b), Ice-front variation and tidewater behavior on Helheim and Kangerdlugssuaq Glaciers, Greenland, *J. Geophys. Res.*, *113*, F01004, doi:10.1029/2007JF000837.

Katz, R. F., and M. G. Worster (2010), Stability of ice-sheet grounding lines, *P. Roy. Soc. A. Math., Phys.*, *466*, 1597–1620, doi:10.1098/rspa.2009.0434.

Knutti, R., G. Abramowitz, M. Collins, V. Eyring, P. J. Gleckler, B. Hewitson, and L. Mearns (2010a), Good practice guidance paper on assessing and combining multi model climate projections, in *Meeting Report of the Intergovernmental Panel on Climate Change Expert Meeting on Assessing and Combining Multi Model Climate Projections*, edited by T. F. Stocker, et al., p. 13, IPCC Working Group I Technical Support Unit, University of Bern, Bern, Switzerland.

Knutti, R., R. Furrer, C. Tebaldi, J. Cermak, and G. A. Meehl (2010b), Challenges in combining projections from multiple climate models, *J. Climate*, *23*, 2739–2758, doi:10.1175/2009JCLI3361.1.

Larour, E., H. Seroussi, M. Morlighem, and E. Rignot (2012a), Continental scale, high order, high spatial resolution, ice sheet modeling using the Ice Sheet System Model (ISSM), *J. Geophys. Res.*, *117*, F01022, doi:10.1029/2011JF002140.

Larour, E., J. Schiermeier, E. Rignot, H. Seroussi, and M. Morlighem (2012b), Sensitivity analysis of Pine Island Glacier ice flow using ISSM and DAKOTA, *J. Geophys. Res.*, *117*, F02009, doi:10.1029/2011JF002146.

Le Brocq, A. M., A. J. Payne, and A. Vieli (2010), An improved Antarctic dataset for high resolution numerical ice sheet models (ALBMAP v1), *Earth Syst. Sci. Data*, *2*, 247–260, doi:10.5194/essd-2-247-2010.

Levermann, A., T. Albrecht, R. Winkelmann, M. A. Martin, M. Haseloff, and I. Joughin (2012), Kinematic first-order calving law implies potential for abrupt ice-shelf retreat, *Cryosphere*, *6*(2), 273–286, doi:10.5194/tc-6-273-201210.

Lipscomb, W., R. Bindschadler, E. Bueler, D. Holland, J. Johnson, and S. Price (2009), A community ice sheet model for sea level prediction, *Eos Trans.*, *90*(3), 23.

Little, C. M., et al. (2007), Toward a new generation of ice sheet models, *Eos Trans.*, *88*, 578.

MacAyeal, D. (1989), Large-scale ice flow over a viscous basal sediment: Theory and application to ice stream B, Antarctica, *J. Geophys. Res.*, *94*(B4), 4071–4087.

Martin, M. A., R. Winkelmann, M. Haseloff, T. Albrecht, E. Bueler, C. Khroulev, and A. Levermann (2011), The Potsdam Parallel Ice Sheet Model (PISM-PIK). Part 2: Dynamic equilibrium simulation of the Antarctic ice sheet, *Cryosphere*, *5*, 727–740, doi:10.5194/tc-5-727-2011.

Mayer, C., and P. Huybrecht (1999), Ice-dynamic conditions across the grounding zone, Ekstromisen, East Antarctica, *J. Glaciol.*, *45*, 384–393.

Mercer, J. H. (1978), West Antarctic ice sheet and CO2 greenhouse effect: A threat of disaster, *Nature*, *271*, 321–325, doi:10.1038/271321a0.

Morland, L. W. (1984), Thermomechanical balances of ice sheet flows, *Geophys. Astrophys. Fluid Dyn.*, *29*, 237–266.

Morland, L. W. (1987), Unconfined ice-shelf flow, in *Dynamics of the West Antarctic Ice Sheet*, edited by C. J. Van der Veen, and J. Oerlemans, pp. 99–116, D. Reidel, Dordretch.

Morlighem, M., E. Rignot, H. Seroussi, E. Larour, H. Ben Dhia, and D. Aubry (2010), Spatial patterns of basal drag inferred using control methods from a full-Stokes and simpler models for Pine Island Glacier, West Antarctica, *Geophys. Res. Lett.*, *37*, L14502, doi:10.1029/2010GL043853.

Nowicki, S. M. J., and D. J. Wingham (2008), Conditions for a steady ice sheet-ice shelf junction, *Earth Planet. Sci. Lett.*, doi:10.1016/j.epsl.2007.10.018.

Nowicki, S. M. J., et al. (2013), Insights into spatial sensitivities of ice mass response to environmental change from the SeaRISE ice sheet modeling project II: Greenland, *J. Geophys. Res. Earth Surf.*, *118*, doi:10.1002/jgrf.20076.

Oppenheimer, M., et al. (2007), Report of the Workshop on Ice Sheet Modeling at the NOAA Geophysical Fluid Dynamics Laboratory 8 January 2007, NOAA and Woodrow Wilson School of Public and International Affairs at Princeton University, 1–7.

Parizek, B. R., and R. T. Walker (2010), Implications of initial conditions and ice-ocean coupling For grounding-line evolution, *Earth Planet. Sci. Lett.*, *300*, 351–358.

Parizek, B. R., R. B. Alley, T. K. Dupont, R. T. Walker, and S. Anandakrishnan (2010), Effect of orbital-scale climate cycling and meltwater drainage on ice sheet grounding line migration, *J. Geophys. Res.*, *115*, F01011, doi:10.1029/2009JF001325.

Parizek, B. R., et al. (2013), Dynamic (in)stability of Thwaites Glacier, West Antarctica, *J. Geophys. Res. Earth Surf. 118*, 1–18, doi:10.1002/jgrf.20044.

Pattyn, F., A. Huyghe, S. D. Brabander, and B. D. Smedt (2006), The role of transition zones in marine ice sheet dynamics, *J. Geophys. Res.*, *111*, F02004, doi:10.1029/2005JF000394.

Pattyn, F., et al. (2012), Results of the Marine Ice Sheet Model Intercomparison Project, MISMIP, *Cryosphere*, *6*, 573–588, doi:10.5194/tc-6-573-2012.

Pattyn, F., et al. (2013), Grounding-line migration in plan-view marine ice-sheet models: Results of the ice2sea MISMIP3d intercomparison, *J. Glaciol.*, *59*(215), 410–422, doi:10.3189/2013JoG12J129.

Payne, A. J., A. Vieli, A. P. Shepherd, D. J. Wingham, and E. Rignot (2004), Recent dramatic thinning of largest West Antarctic ice stream triggered by oceans, *Geophys. Res. Lett.*, *31*, L23401, doi:10.1029/2004GL021284.

Payne, A. J., P. R. Holland, A. P. Shepherd, I. C. Rutt, A. Jenkins, and I. Joughin (2007), Numerical modeling of ocean-ice interactions under Pine Island Bay's ice shelf, *J. Geophys. Res.*, *112*, C10019, doi:10.1029/2006JC003733.

Peters, M. E., D. D. Blankenship, and D. L. Morse (2005), Analysis techniques for coherent airborne radar sounding, *J. Geophys. Res.*, *110*, B06303, doi:10.1029/2004JB003222.

Petit, J. R., et al. (1999), Climate and atmospheric history of the past 420,000 years from the Vostok ice core, Antarctica, *Nature*, *399*, 429–436.

Pollard, D., and R. M. DeConto (2009), Modelling West Antarctic ice sheet growth and collapse through the past five million years, *Nature*, *458*, 329–332.

Pollard, D., and R. DeConto (2012), Description of a hybrid ice sheet-shelf model, and application to Antarctica, *Geosci. Mod. Develop. Disc.*, *5*, 1077–1134.

Price, S. F., A. J. Payne, I. M. Howat, and B. E. Smith (2011), Committed sea-level rise for the next century from Greenland ice sheet dynamics during the past decade, *Proc. Nat. Acad. Sci.*, *108*, 8978–8983.

Pritchard, H. D., S. R. M. Ligtenberg, H. A. Fricker, D. G. Vaughan, M. R. van den Broeke, and L. Padman (2012), Antarctic ice-sheet loss driven by basal melting of ice shelves, *Nature*, *484*, doi:10.1038/nature10968.

Reeh, N. (1991), Parameterization of melt rate and surface temperature on the Greenland ice sheet, *Polarforschung*, *59*(3), 113-128.

Rignot, E. (2008), Changes in West Antarctic ice stream dynamics observed with ALOS PALSAR data, *Geophys. Res. Lett.*, *35*, L12505, doi:10.1029/2008GL033365.

Rignot, E., J. Mouginot, and B. Scheuchl (2011), Ice flow of the Antarctic Ice Sheet, *Science*, *333*, 1427–1430, doi:10.1126/science.1208336.

Rogelj, J., M. Meinshausen, and R. Knutti (2012), Global warming under old and new scenarios using IPCC climate sensitivity range estimates, *Nat. Clim. Change*, *2*, 248–253, doi:10.1038/nclimate1385.

Rogozhina, I., Z. Martinec, J. M. Hagedoorn, M. Thomas, and K. Fleming (2011), On the long term memory of the Greenland Ice Sheet, *J. Geophys. Res.*, *116*, F01011, doi:10.1029/2010JF001787.

Sanderson, T. J. O. (1979), Equilibrium profile of ice shelves, *J. Glaciol.*, *22*(88), 435–460.

Sato, T., and R. Greve (2012), Sensitivity experiments for the Antarctic ice sheet with varied sub-ice-shelf melting rates, *Ann. Glaciol.*, *53*, 221–228.

Scambos, T. A., J. Bohlander, C. Shuman, and P. Skvarca (2004), Glacier acceleration and thinning after ice shelf collapse in the Larsen B embayment, Antarctica, *Geophys. Res. Lett.*, *31*, L18402, doi:10.1029/2004GL020670.

Scambos, T., H. A. Fricker, C.-C. Liu, J. Bohlander, J. Fastook, A. Sargent, R. Massom, and A.-M. Wu (2009), Ice shelf disintegration by plate bending and hydro-fracture: Satellite observations and model results of the 2008 Wilkins ice shelf break-ups, *Earth Planet. Sci. Lett.*, *280*, 51–60, doi:10.1016/j.epsl.2008.12.027.

Schoof, C. (2007a), Ice sheet grounding line dynamics: Steady states, stability, and hysteresis, *J. Geophys. Res.*, *112*, F03S28, doi:10.1029/2006JF000664.

Schoof, C. (2007b), Marine ice sheet dynamics. Part 1: The case of rapid sliding, *J. Fluid Mech.*, *573*, 27–55.

Schoof, C., and R. C. A. Hindmarsh (2010), Thin-film flows with wall slip: an asymptotic analysis of higher order glacier flow models, *Quart. J. Mech. Appl. Math.*, *63*(1), 73–114, doi:10.1093/qjmam/hbp025.

Schoof, C. (2011), Marine ice sheet dynamics. Part 2: A Stokes Flow contact problem, *J. Fluid Mech.*, *679*, 122–255.

Seddik, H., R. Greve, T. Zwinger, F. Gillet-Chaulet, and O. Gagliardini (2012), Simulations of the Greenland ice sheet 100 years into the future with the full Stokes model Elmer/Ice, *J. Glaciol.*, *58*, 427–440.

Seroussi, H., M. Morlighem, E. Rignot, E. Larour, D. Aubry, H. Ben Dhia, and S. S. Kristensen (2011), Ice flux divergence anomalies on 79north Glacier, Greenland, *Geophys. Res. Lett.*, *38*, L09501, doi:10.1029/2011GL047338.

Shapiro, N. M., and M. H. Ritzwoller (2004), Inferring surface heat flux distributions guided by a global seismic model: Particular application to Antarctica, *Earth Planet. Sci. Lett.*, *223*, 213–224.

Shepherd, A., D. J. Wingham, and E. Rignot (2004), Warm ocean is eroding West Antarctic Ice Sheet, *Geophys. Res. Lett.*, *31*, L23402, doi:10.1029/2004GL021106.

Stearns, L. A., and G. S. Hamilton (2007), Rapid volume loss from two East Greenland outlet glaciers quantified using repeat stereo satellite imagery, *Geophys. Res. Lett.*, *34*, L05503, doi:10.1029/2006GL028982.

Stephenson, D. B., C. A. S. Coelho, F. J. Doblas-Reyes, and M. Balmaseda (2005), Forecast assimilation: A unified framework for the combination of multi-model weather and climate predictions, *Tellus A*, *57*, 253–264.

Stone, E., D. Lunt, I. Rutt, and E. Hanna (2010), Investigating the sensitivity of numerical model simulations of the modern state of the Greenland ice-sheet and its future response to climate change, *Cryosphere*, *4*, 397–417.

Thomas, R. H. (1973), The creep of ice shelves: Theory, *J. Glaciol.*, *12*(64), 45–53.

Thomas, R. H. (1979), The dynamics of marine ice sheets, *J. Glaciol.*, *24*(90), 167–177.

Timmermann, R., A. Beckmann, and H. H. Hellmer (2002), Simulation of ice-ocean dynamics in the Weddell Sea. Part I: Model configuration and validation, *J. Geophys. Res.*, *107*(C3), 3024, doi:10.1029/2000JC000741.

Vaughan, D. G., and R. J. Arthern (2007), Why is it hard to predict the future of ice sheets? *Science*, *315*, 1503–1504, doi:10.1126/science.1141111.

Vaughan, D. V., J. L. Bamber, M. Giovinetto, J. Russell, and A. P. R. Cooper (1999), Reassessment of net surface mass balance in Antarctica, *J. Clim.*, *12*, 933–946.

van der Veen, C. J., and ISMASS (2010), Ice sheet mass balance and sea level: A science plan, SCAR Report 38, July 2010, ISSN 1755–9030, 35p.

van der Veen, C. J., and A. J. Payne (2004), Modelling land-ice dynamics, in *Mass Balance of the Cryosphere Observations and Modelling of Contemporary and Future Changes*, edited by J. L. Bamber, and A. J. Payne, pp. 169–219, Cambridge University Press, Cambridge UK.

Vieli, A., and F. M. Nick (2011), Understanding and modelling rapid dynamic changes of tidewater outlet glaciers: Issues and implications, *Surv. Geophys.*, *32*, 437–458.

Vieli, A., and A. J. Payne (2005), Assessing the ability of numerical ice sheet models to simulate grounding line migration, *J. Geophys. Res.*, *110*, F01003, doi:10.1029/2004JF000202.

Walker, R. T., T. K. Dupont, B. R. Parizek, and R. B. Alley (2008), Effects of basal-melting distribution on the retreat of ice-shelf grounding lines, *Geophys. Res. Lett.*, *35*, L17503, doi:10.1029/2008GL034947.

Wang, W., J. Li, and J. Zwally (2012), Dynamic inland propagation of thinning due to ice loss at the margins of the Greenland ice sheet, *J. Glaciol.*, *58*, 734–740.

Weertman, J. (1957), Deformation of floating ice shelves, *J. Glaciol.*, *3*, 38–42.

Weertman, J. (1974), Stability of the junction of an ice sheet and an ice shelf, *J. Glaciol.*, *13*(67), 3–11.

Weigel, A. P., R. Knutti, M. A. Liniger, and C. Appenzeller (2010), Risks of model weighting in multimodel climate projections, *J. Climate*, *23*(15), 4175–4191.

Williams, M. J. M., K. Grosfeld, R. C. Warner, R. Gerdes, and J. Determann (2001), Ocean circulation and ice-ocean interaction beneath the Amery Ice Shelf, Antarctica, *J. Geophys. Res.*, *106*(C10), 22383–22399.

Winkelmann, R., M. A. Martin, M. Haseloff, T. Albrecht, E. Bueler, C. Khroulev, and A. Levermann (2011), The Potsdam Parallel Ice Sheet Model (PISM-PIK). Part 1: Model description, *Cryosphere*, *5*, 715–726, doi:10.5194/tc-5-715-2011.